

Coulomb interactions, Dirac sea polarization and $SU(4)$ symmetry breaking of the integer quantum Hall states of graphene

Vinu Lukose* and R. Shankar†
The Institute of Mathematical Sciences,
C.I.T. Campus, Taramani, Chennai 600 113, India
 (Dated: March 6, 2022)

We investigate effects of the filled Dirac sea on the $SU(4)$ symmetry breaking in the integer quantum Hall states of graphene with long-ranged Coulomb interactions. Our model also includes Hubbard and nearest neighbour repulsive interactions with strengths U and V respectively. We find that the symmetry breaking of the $n = 0$ Landau levels induces an $SU(4)$ polarization of the Dirac sea. This results in several phases which are absent when the effects of the Dirac sea are neglected. We compute the phase diagram in the U - V space. We also calculate the excitation gaps in tilted magnetic fields for all the phases. We compare our model results with experiments and find a range of U and V that are consistent with them.

PACS numbers: 73.43.Cd

I. INTRODUCTION

Graphene¹ has given access to a truly two dimensional electronic gas. The low energy physics for graphene is governed by the four species of Dirac quasi-particles leading to an emergent $SU(4)$ symmetry. Dirac particles of the low energy and the long wavelength theory were predicted² to have an unusual sequence of quantum Hall plateaus for graphene, $\sigma_H = 4(n + 1/2)e^2/h$ and it was observed^{3,4}. The charge neutral point of graphene in a magnetic field is the filled Dirac sea of quartets of Landau levels with index $n < 0$ and half-filled quartet of the $n = 0$ Landau level. The orbital degeneracy of each member of the quartet is always saturated in this article. The Dirac sea manifests in the non-interacting model in the unusual form of the Hall conductivity mentioned above.

High mobility graphene samples on boron nitride unveiled plateaus at all integer values⁵ indicating that the $SU(4)$ symmetry is spontaneously broken. The theory for the $SU(4)$ symmetry breaking near the charge neutral point has been addressed in past⁶⁻¹⁶. The long-ranged Coulomb interaction was shown to break the $SU(4)$ symmetry spontaneously⁶ and it was predicted that the Hall plateaus should reveal for all integer values. The interactions can be written as a sum of $SU(4)$ symmetric long-ranged Coulomb part and short-ranged symmetry breaking parts. The long-ranged Coulomb interaction results in the spontaneous breaking of the $SU(4)$ symmetry. The pattern of symmetry breaking is $U(4) \rightarrow U(m) \times U(4 - m)$ ⁷, where $m < 4$ is the number of members of the quartet of occupied Landau level with the highest energy. The ground state manifold is the coset space $U(4)/(U(m) \times U(4 - m))$.

The symmetry breaking terms pick out a state (or states) in the ground state manifold. The short-ranged interaction and the Zeeman terms play an important role in deciding the nature of the ground state at Hall conductivities $\sigma_H = 0, \pm 1$. The ground state at $\sigma_H = \pm 1$ was shown to be a valley-spin polarized state⁸. The ground state at $\sigma_H = 0$, there are various possibilities: charge

ordered state^{8,12-14}, anti-ferromagnetic state^{12,13}, canted anti-ferromagnetic state^{13,16} and Kekule ordering¹³. The filled Dirac sea of Landau levels with the short-ranged interaction terms were first included in the computation of ground state energies by Herbut¹².

In all these works, the effects of the long-ranged Coulomb interaction of the Dirac sea and the consequences for the $SU(4)$ symmetry breaking have not been investigated. We expect the long-ranged Coulomb interactions to significantly affect the structure of the Dirac sea. In this paper we take up this technically challenging problem of including the Dirac sea with the Coulomb interactions.

We start with a realistic model on the lattice that includes the Coulomb interaction between the point charges as well as the on-site and the nearest-neighbour repulsion to account for the finite extent of the wavefunctions. We perform a systematic long wavelength expansion and derive the effective low energy continuum model. This model consists of an $SU(4)$ symmetric part and $SU(4)$ breaking terms. The symmetric part includes the kinetic term and the long-ranged Coulomb interactions. The symmetry breaking part consists of short-ranged interaction terms and the Zeeman term and these are suppressed by a factor of a/ℓ_c with respect to the symmetric terms, where a is the graphene lattice constant and $\ell_c \equiv \sqrt{\hbar/eB}$, is the magnetic length.

Since we are interested in the regime where $a/\ell_c \ll 1$, we adopt the strategy of approximately solving the symmetric part using the variational method and then treating the symmetry breaking terms in first order perturbation theory. The variational state we choose is the ground state of a quartet of Dirac particles in the background of a mass matrix. The sixteen parameters that specify the hermitian mass matrix are our variational parameters. We develop a method, based on the ‘heat kernel’ representation of the Dirac propagator, which makes the computation of the Coulomb energy tractable.

The picture that emerges from our calculations is the following: consider the non-interacting system with par-

tially filled quartet for the $n = 0$ Landau level and fully filled quartet for the $n < 0$ Landau levels. We will refer to the $n < 0$ occupied Landau levels as the Dirac sea. The Dirac sea is a $SU(4)$ singlet and has all four charges uniformly distributed on the sites. The partially filled quartet of the $n = 0$ Landau level breaks the $SU(4)$ symmetry and the four charges are distributed unequally between the two sublattices of the honeycomb lattice. When the Coulomb interactions are turned on, this induces a redistribution of the charges in the sea, leading to what we call a staggered polarization of the Dirac sea which plays an important role in the nature of the broken symmetry phases. We show that it results in two phases which are absent if this effect is ignored. One is the canted-spin state at $\sigma_H = 0$, which was first discussed in reference [13]. Another is what we call the valley-spin canted phase which occurs at $\sigma_H = -1$, which has not been discussed earlier.

The rest of this paper is organized as follows. In Sec.II we start with a realistic lattice model and motivate the effective continuum interacting model adopted in this paper. Sec.III is a discussion of symmetries of the hamiltonian and the order parameters corresponding to the $SU(4)$ polarization and the staggered polarization. In Sec.IV, we describe the variational wavefunction used to compute the variational energy for the interacting model. Sec.V gives the details of the technical aspects for computing the variational energy that takes into account the filled sea of Landau levels by computing the two point correlators. The two point correlators are used to describe the nature of the polarization of the Dirac sea in Sec.VI. In Sec.VII, we present the results for the symmetric interacting model, i.e. model comprising the kinetic and the long-ranged Coulomb interaction terms. Sec.VIII presents the effect of symmetry breaking terms of our model on the nature of the ground states and the elementary excitations by specifying the $SU(4)$ polarization. In Sec.IX, we compare our results to recent experiments^{5,14} and find that there is a region in our phenomenological parameters, U and V , that is consistent with the experimental results. We conclude with a summary of the main results of the paper in Sec.X.

II. THE INTERACTING MODEL

In this section, we describe the motivation for adopting the interacting continuum model in this article. We start with the lattice model. The hamiltonian is,

$$\mathcal{H} = \mathcal{H}_0 + \mathcal{H}_I, \quad (1)$$

where $\mathcal{H}_0 \equiv \mathcal{H}_t + \mathcal{H}_Z$, is the non-interacting model for graphene in a magnetic field which includes the tight binding term, \mathcal{H}_t and the Zeeman term, \mathcal{H}_Z . $\mathcal{H}_I \equiv \mathcal{H}_{\tilde{C}} + \mathcal{H}_{\tilde{V}} + \mathcal{H}_U$, is the interaction term. $\mathcal{H}_{\tilde{C}}$ is the Coulomb interaction between a pair of point charges on lattice sites. The finite extent of the electron wavefunctions modify the interaction at short distances. This is

taken into account by including the repulsive interactions with the nearest neighbour ($\mathcal{H}_{\tilde{V}}$) and the on-site Hubbard term (\mathcal{H}_U)^{8,12,13}. The strengths of the nearest neighbour and the Hubbard interactions are treated as phenomenological parameters in our analysis.

We review the tight binding model for graphene and describe the systematic long wavelength expansion around the Dirac points for the lattice operators. The leading derivative term obtained after continuum approximation is the well-studied Dirac hamiltonian of the non-interacting model. We apply continuum approximation to lattice interaction terms. The leading term is $SU(4)$ symmetric and long-ranged. The sub-leading terms break the $SU(4)$ symmetry explicitly and the interactions are short-ranged.

A. The continuum theory

The tight binding model in the absence of magnetic field for graphene describes the nearest neighbour hopping of the π -electrons of carbon atoms. The lattice hamiltonian is,

$$\mathcal{H}_t = -t \sum_{\mathbf{n}, \sigma} c_{1, \sigma, \mathbf{n}}^\dagger \left(\sum_{j=1}^3 c_{2, \sigma, \mathbf{n} + \mathbf{b}_j} \right) + \text{h.c.} \quad (2)$$

Here $t \approx 3 \text{ eV}$, is the hopping parameter. $c_{r, \sigma, \mathbf{n}}$ are the electron annihilation operators. \mathbf{n} labels the triangular lattice sites and $r = 1, 2$ the sublattices. $\sigma = \uparrow, \downarrow$, is the spin index. The three vectors, \mathbf{b}_j , $j = 1, 2, 3$, are equal to $0, \mathbf{e}_2$ and $\mathbf{e}_1 + \mathbf{e}_2$, where \mathbf{e}_1 and \mathbf{e}_2 are the basis vectors for the triangular lattice. The electron creation and annihilation operators obey the canonical anti-commutation relation, $\{c_{r, \sigma, \mathbf{n}}, c_{\tilde{r}, \tilde{\sigma}, \tilde{\mathbf{n}}}^\dagger\} = \delta_{r, \tilde{r}} \delta_{\sigma, \tilde{\sigma}} \delta_{\mathbf{n}, \tilde{\mathbf{n}}}$.

At half filling, the Fermi level of the tight binding model for graphene is at zero. There are two points in the Brillouin zone with zero energy where the two bands touch: the Dirac points, $\mathbf{K}_\pm = (\pm 2\pi/3a, \pm 2\pi/3a)$. Near the Dirac points, the quasi-particle energies have a linear dispersion relation.

To obtain the low energy effective theory from the lattice hamiltonian, we project the electron operators to small regions around the Dirac points. Separating the long wavelength modes from the fast varying modes, we can write,

$$c_{r, \sigma, \mathbf{n}} \approx a \left(e^{i\mathbf{K}_+ \cdot \mathbf{n}} \beta_{r, s} \Psi_{s, +, \sigma}(\mathbf{n}) + e^{i\mathbf{K}_- \cdot \mathbf{n}} \alpha_{r, s}^x \Psi_{s, -, \sigma}(\mathbf{n}) \right). \quad (3)$$

a is the lattice spacing. $\alpha^x, \alpha^y, \alpha^z \equiv \beta$, are the Pauli matrices. $\Psi_{r, \eta, \sigma}(\mathbf{n})$ are the slow varying modes around the two Dirac points. $\eta = \pm$, is the valley index, labeling the states around the Dirac points \mathbf{K}_\pm .

The leading term from continuum approximation of the lattice kinetic term, Eq.(2), then becomes:

$$\mathcal{H}_t = \int d\mathbf{x} \Psi^\dagger(\mathbf{x}) \left(v_F \boldsymbol{\alpha} \cdot \mathbf{p} \otimes \mathbb{1}_4 \right) \Psi(\mathbf{x}). \quad (4)$$

This non-interacting hamiltonian describes four species of free massless Dirac particles. The speed of the massless particle is $v_F = \sqrt{3} a t / 2 \hbar$, the Fermi velocity at the Dirac point. The field operators, $\Psi(\mathbf{x})$ are eight component objects and are labeled as $\Psi_{r,A}(\mathbf{x})$, where r refers to the Dirac spinor or sublattice index taking values $r = 1, 2$. The spin and valley indices are combined into the $SU(4)$ index, A , which takes values $1, \dots, 4$.

For weak magnetic fields, $a/\ell_c \ll 1$, the vector potential can be chosen to be slowly varying on the scale of lattice spacing and the continuum approximation of the lattice kinetic term is,

$$\mathcal{H}_t = \kappa_t \int d\mathbf{x} \Psi^\dagger(\mathbf{x}) (\boldsymbol{\alpha} \cdot \boldsymbol{\pi} \otimes \mathbb{1}_4) \Psi(\mathbf{x}). \quad (5)$$

Here $\boldsymbol{\pi} = \mathbf{p} - e\mathbf{A}$ and \mathbf{A} is the vector potential. We have chosen dimensionless variables by the scaling,

$$\mathbf{x} \rightarrow \ell_c \mathbf{x}, \quad \boldsymbol{\pi} \rightarrow \frac{\hbar}{\ell_c} \boldsymbol{\pi}, \quad \Psi(\mathbf{x}) \rightarrow \frac{1}{\ell_c} \Psi(\mathbf{x}).$$

The parameter, κ_t has a square root dependence on the perpendicular component of the magnetic field, B_\perp ,

$$\kappa_t = \frac{\hbar v_F}{\ell_c}. \quad (6)$$

In the presence of a magnetic field, the lattice Zeeman term is,

$$\mathcal{H}_Z = -g \frac{\mu_B}{\hbar} \sum_{\mathbf{n}} \sum_r \mathbf{B} \cdot \mathbf{S}_{r,\mathbf{n}}. \quad (7)$$

The spin operator in terms of the lattice fermion operators is, $S_{r,\mathbf{n}}^j = (\hbar/2) c_{r,\mathbf{n}}^\dagger \sigma^j c_{r,\mathbf{n}}$. The continuum approximation results in a term that breaks the spin rotation symmetry,

$$\mathcal{H}_Z = -\kappa_Z \int_{\mathbf{x}} \Psi^\dagger(\mathbf{x}) \boldsymbol{\sigma} \cdot \mathbf{B} \Psi(\mathbf{x}). \quad (8)$$

The parameter, κ_Z , depends on the total magnetic field, B_T (Tesla),

$$\kappa_Z = \frac{1}{2} g \mu_B B_T = 0.67 B_T K. \quad (9)$$

B. Interaction terms

The electron-electron interaction for graphene lattice is modeled by combining the Coulomb point charge interaction, $\mathcal{H}_{\tilde{C}}$, the short-ranged nearest neighbour interaction, $\mathcal{H}_{\tilde{V}}$, and the on-site Hubbard interaction, \mathcal{H}_U ,

$$\mathcal{H}_I = \mathcal{H}_{\tilde{C}} + \mathcal{H}_{\tilde{V}} + \mathcal{H}_U. \quad (10)$$

The lattice Coulomb interaction is,

$$\mathcal{H}_{\tilde{C}} = \frac{1}{2} \sum_{\mathbf{n}, \mathbf{m}} \sum_{r,s} \hat{n}_{r,\sigma,\mathbf{n}} V(|\mathbf{n}_r - \mathbf{m}_s|) \hat{n}_{s,\tilde{\sigma},\mathbf{m}}. \quad (11)$$

Here $|\mathbf{n}_r - \mathbf{m}_s|$ is the distance between the two sub-lattice points under consideration, and $V(|\mathbf{r}|) = e^2 / (4\pi\epsilon |\mathbf{r}|)$. $\epsilon = \epsilon_0 \epsilon_r$, where ϵ_r is dielectric constant. And there is a constraint on summation: $r \neq s$ when $\mathbf{n} = \mathbf{m}$.

The interaction effects due to the finite extent of the wavefunctions at short distances are taken into account by including the nearest neighbour interaction term,

$$\mathcal{H}_{\tilde{V}} = \tilde{V} \sum_{\mathbf{n}, \sigma, \tilde{\sigma}} \hat{n}_{1,\sigma,\mathbf{n}} \left(\sum_{j=1}^3 \hat{n}_{2,\tilde{\sigma},\mathbf{n}+\mathbf{b}_j} \right). \quad (12)$$

and the Hubbard term,

$$\mathcal{H}_U = U \sum_{\mathbf{n}} \sum_r \hat{n}_{r,\uparrow,\mathbf{n}} \hat{n}_{r,\downarrow,\mathbf{n}}. \quad (13)$$

The leading a/ℓ_c term after continuum approximation for the Coulomb interaction term, Eq.(11), is $SU(4)$ symmetric,

$$\mathcal{H}_C = \kappa_C \int_{\mathbf{x}, \mathbf{y}} \frac{1}{|\mathbf{r}|} \rho(\mathbf{x}) \rho(\mathbf{y}). \quad (14)$$

Here $\rho(\mathbf{x}) = \Psi^\dagger(\mathbf{x}) \Psi(\mathbf{x})$, is the charge density operator and $|\mathbf{r}| = |\mathbf{x} - \mathbf{y}|$. The parameter κ_C , has $\sqrt{B_\perp}$ dependence and is inversely proportional to the dielectric constant,

$$\kappa_C = \frac{1}{2} \frac{e^2}{4\pi\epsilon\ell_c}. \quad (15)$$

There are sub-leading terms which become significant at short distances because of inverse cube (and higher power) dependence on the distance. They break the $SU(4)$ symmetry explicitly. This symmetry breaking pattern is similar to continuum approximation of the nearest neighbour interaction term, Eq.(12). In our continuum model, we combine these symmetry breaking terms into \mathcal{H}_V with a new parameter V .

$$\mathcal{H}_V = \kappa_V \int_{\mathbf{x}} \left((\rho(\mathbf{x}))^2 - (\Psi^\dagger(\mathbf{x}) \beta \tau^z \Psi(\mathbf{x}))^2 \right). \quad (16)$$

This approximation forgoes the distance variation of terms with higher order in a/ℓ_c for the point charge interaction, Eq.(11), but retains the essential physics of $SU(4)$ symmetry breaking. This approximation simplifies our variational energy computation immensely.

The continuum approximation of the Hubbard term in manifestly spin invariant form yields the following set of local interaction terms,

$$\mathcal{H}_U = \kappa_U \int_{\mathbf{x}} \left((\rho(\mathbf{x}))^2 + (\Psi^\dagger(\mathbf{x}) \beta \tau^z \Psi(\mathbf{x}))^2 + \frac{1}{2} \sum_{j,k=x,y} (\Psi^\dagger(\mathbf{x}) \alpha^j \tau^k \Psi(\mathbf{x}))^2 \right). \quad (17)$$

The tight binding term, Eq.(2), results in a series of sub-leading terms after continuum approximation. These

κ_t	$\frac{\hbar v_F}{\ell_c^2}$	$0.86t\left(\frac{a}{\ell_c}\right)$
κ_C	$\frac{1}{2} \frac{e^2}{4\pi\epsilon\ell_c}$	$\frac{5.82}{\epsilon_r} \left(\frac{a}{\ell_c}\right)$
κ_Z	$\frac{g\mu_B B}{2}$	$0.63\left(\frac{a}{\ell_c}\right)^2$
κ_V	$\frac{3Va^2}{4\ell_c^2}$	$0.75V\left(\frac{a}{\ell_c}\right)^2$
κ_U	$\frac{Ua^2}{4\ell_c^2}$	$0.25U\left(\frac{a}{\ell_c}\right)^2$
κ_{t_1}	$\frac{ta^2}{8\ell_c^2}$	$0.125t\left(\frac{a}{\ell_c}\right)^2$

TABLE I. The first two columns list and define all the energy parameters in the interacting model. In the third column, we explicitly express the parameters as function of a/ℓ_c in units of eV . For the magnetic fields typically achieved in a laboratory, $a/\ell_c \sim 10^{-1}$ to 10^{-2} , a small parameter. The kinetic and Coulomb energy parameters are dominant and the remaining ones are smaller by a factor of a/ℓ_c .

terms involve higher order derivatives. The first of such sub-leading terms is,

$$\mathcal{H}_{t_1} = \kappa_{t_1} \int d\mathbf{x} \Psi^\dagger(\mathbf{x}) h_{t_1} \Psi(\mathbf{x}), \quad (18)$$

with $h_{t_1} = (\alpha^x(\pi_x^2 + 3\pi_y^2) - \alpha^y 3(\pi_x\pi_y + \pi_y\pi_x)) \otimes \tau^z$.

The parameters,

$$\kappa_V = \frac{3Va^2}{4\ell_c^2}, \quad \kappa_U = \frac{Ua^2}{4\ell_c^2}, \quad \kappa_{t_1} = \frac{ta^2}{8\ell_c^2}. \quad (19)$$

have linear dependence on B_\perp . We treat both V and U as phenomenological parameters for our interacting continuum model.

To summarize, the continuum interacting model hamiltonian that we use in this article is,

$$\mathcal{H} = \mathcal{H}_0 + \mathcal{H}_1. \quad (20)$$

$$\mathcal{H}_0 = \mathcal{H}_t + \mathcal{H}_C. \quad (21)$$

$$\mathcal{H}_1 = \mathcal{H}_V + \mathcal{H}_U + \mathcal{H}_Z + \mathcal{H}_{t_1}. \quad (22)$$

\mathcal{H}_0 , defined in Eq.(5) and Eq.(14), is the $SU(4)$ symmetric term. \mathcal{H}_1 defined in Eq.(16), Eq.(17), Eq.(8) and Eq.(18), is the symmetry breaking term. The a/ℓ_c dependence of the coefficients in Table I shows that \mathcal{H}_0 is the leading order term and \mathcal{H}_1 is smaller by a factor of a/ℓ_c .

Our strategy is to approximately solve \mathcal{H}_0 using the variational method. As we will see, this leads to $SU(4)$ symmetry broken ground state solutions which are degenerate. We then treat \mathcal{H}_1 in first order perturbation theory to see which ground state(s) is (are) picked out by the energetics.

III. SYMMETRIES AND ORDER PARAMETERS

In this section, we discuss the details of the $SU(4)$ symmetry displayed by various terms of our interacting model. We also discuss various order parameters for the ground states.

A. The $SU(4)$ symmetry

Under $SU(4)$ transformations, the fermion field operator transforms as,

$$\tilde{\Psi}_{r,A}(\mathbf{x}) = \mathcal{U}_{A,B} \Psi_{r,B}(\mathbf{x}), \quad (23)$$

where $\mathcal{U} \in SU(4)$. As mentioned earlier, \mathcal{H}_0 is invariant under this transformation.

\mathcal{H}_1 breaks this $SU(4)$ symmetry. The short-ranged interactions, \mathcal{H}_V and \mathcal{H}_U , are invariant under transformations belonging to the subgroup, $U(1) \times SU(2)$, i.e.

$$\mathcal{U} = e^{-\frac{i}{2}\theta_\tau \tau^z} \otimes U_\sigma. \quad (24)$$

Here U_σ denotes a unitary rotation in $SU(2)$ spin space. There is also a discrete symmetry that leaves the short-ranged interactions invariant,

$$\mathcal{U} = \tau^x \otimes U_\sigma. \quad (25)$$

This transformation amounts to interchanging the valley indices of the field operators. The group that leaves the short-ranged interaction terms invariant is a semi-direct product of $Z_2 \rtimes U(1) \otimes SU(2)$.

The sub-leading correction to the kinetic term, \mathcal{H}_{t_1} , given in Eq.(18), is only invariant under $U(1) \otimes SU(2)$.

The Zeeman term, \mathcal{H}_Z , breaks the $SU(2)$ spin symmetry to $U(1)$.

$$\mathcal{U} = U_\tau \otimes e^{-\frac{i}{2}\theta_\sigma \sigma^z}, \quad (26)$$

is the transformation of the field operator that leaves the Zeeman term invariant. Here U_τ is a unitary rotation in $SU(2)$ valley space.

The model hamiltonian, Eq.(20), is invariant under $U(1) \times U(1)$ rotation. The transformation

$$\mathcal{U} = e^{-\frac{i}{2}\theta_\tau \tau^z} \otimes e^{-\frac{i}{2}\theta_\sigma \sigma^z}, \quad (27)$$

of the field operators leaves \mathcal{H} invariant.

B. Order parameters

$U(4)$ has sixteen generators. They can be represented by the 4×4 matrices, $T^{\mu\nu} \equiv \tau^\mu \otimes \sigma^\nu$, $\mu, \nu = 0, x, y, z$, where we define τ^0 and σ^0 to be 2×2 identity matrices.

The operators representing the $U(4)$ charge densities are $\mathcal{T}^{\mu\nu}(\mathbf{x}) \equiv \Psi^\dagger(\mathbf{x}) T^{\mu\nu} \Psi(\mathbf{x})$. The ground state expectation value, $\langle \mathcal{T}^{\mu\nu}(\mathbf{x}) \rangle$, correspond to the $SU(4)$ polarization of the ground state.

There are also sixteen other order parameters that can be constructed, $\tilde{\mathcal{T}}^{\mu\nu}(\mathbf{x}) \equiv \Psi^\dagger(\mathbf{x}) \beta \otimes T^{\mu\nu} \Psi(\mathbf{x})$. These two types of operators can be distinguished by their transformation properties under reflection,

$$\Psi(x, y) \rightarrow i\alpha^y \Psi(-x, y). \quad (28)$$

Under this transformation, we have

$$\mathcal{T}^{\mu\nu}(x, y) \rightarrow \mathcal{T}^{\mu\nu}(-x, y), \quad \tilde{\mathcal{T}}^{\mu\nu}(x, y) \rightarrow -\tilde{\mathcal{T}}^{\mu\nu}(-x, y).$$

The operation of α^y switches the Dirac indices, corresponding to a switch of the sublattice index. We refer to the expectation values of these operators that are odd under this transformation, as the staggered $SU(4)$ polarization of the ground state.

In Appendix C, we have given a list of lattice operators corresponding to each of the 32 order parameters we have discussed above. Note that many lattice operators can have the same continuum limit. We have listed the simplest representative lattice operator.

Some of the operators are linear combinations of the products of electron operators on the same lattice site. $\mathcal{T}^{00}(\mathbf{x})$ is the total charge density in the unit cell and $\mathcal{T}^{0i}(\mathbf{x})$ the total spin density. $\tilde{\mathcal{T}}^{30}(\mathbf{x})$ is the charge density wave order parameter corresponding to the difference in charge densities on the two sublattice points in the unit cell and $\tilde{\mathcal{T}}^{3i}(\mathbf{x})$ is the Neel order parameter corresponding to the difference in spin densities on the two sublattices.

The operator $\tilde{\mathcal{T}}^{00}(\mathbf{x})$ is a time-reversal symmetry breaking mass term. It is the continuum limit of the operator that occurs in Haldane's model¹⁷ of a Chern insulator on the honeycomb lattice. Thus $\tilde{\mathcal{T}}^{0\nu}(\mathbf{x})$ are all bond-order parameters at the lattice level.

The operators involving τ^x or τ^y transfer particles from $\mathbf{K}_+ \leftrightarrow \mathbf{K}_-$. The corresponding lattice operators hence involve a momentum transfer of $\pm(\mathbf{K}_+ - \mathbf{K}_-)$.

IV. VARIATIONAL WAVEFUNCTION

The main aim of this paper is to study the effects of the Dirac sea of Landau levels on the $SU(4)$ symmetry breaking induced by the interactions. To this end, we want to construct variational states such that (i) they allow the $SU(4)$ polarization of the Dirac sea and (ii) the energy computations are tractable.

We investigate a simple family of states that satisfy these two conditions, namely the variational state is constructed using the eigenstates of one-particle Dirac hamiltonian for a quartet of massive particles in the presence of a magnetic field, h_M ,

$$h_M = \boldsymbol{\alpha} \cdot \boldsymbol{\pi} + \beta M. \quad (29)$$

Here M is a 4×4 hermitian mass matrix. It is specified by 16 independent real numbers that we treat as variational parameters.

The eigenvectors of h_M are of the form, $\Phi_{r,A}^{n,l,q}(\mathbf{x}) = \phi_r^{n,l,q}(\mathbf{x}) \chi_A^q$. m_q , $q = 1, \dots, 4$ are the eigenvalues of M and χ^q the corresponding eigenvectors. $\phi_r^{n,l,q}(\mathbf{x})$ are the Landau levels for a $(2+1)d$ massive Dirac particle with mass m_q . We expand the field operators in terms of these

eigenvectors,

$$\Psi_{r,A}(\mathbf{x}) = \sum_{n,l,q} \Phi_{r,A}^{n,l,q}(\mathbf{x}) \psi_{n,l,q}. \quad (30)$$

$\psi_{n,l,q}^\dagger$ is the creation operator for an electron with Landau level index n , orbital degeneracy index l , and $SU(4)$ quantum number q .

The variational ground states are constructed by filling the quartet for Landau levels with index $n \leq -1$, constituting the Dirac sea. The state for $\sigma_H = 0$ has half-filled quartet of the $n = 0$ Landau level and a quarter-filled quartet of the $n = 0$ Landau level for $\sigma_H = -1$. The variational state for $\sigma_H = +1$ is the charge conjugate state of $\sigma_H = -1$, so we are only going to study $\sigma_H = -1$.

$$|\sigma_H = 0\rangle = \left(\prod_{\substack{l=0, \\ q=1}}^{\infty, 2} \psi_{0,l,q}^\dagger \right) \left(\prod_{n=-1}^{-N_c} \prod_{\substack{l=-|n|, \\ q=1}}^{\infty, 4} \psi_{n,l,q}^\dagger \right) |0\rangle. \quad (31)$$

$$|\sigma_H = -1\rangle = \left(\prod_{l=0}^{\infty} \psi_{0,l,1}^\dagger \right) \left(\prod_{n=-1}^{-N_c} \prod_{\substack{l=-|n|, \\ q=1}}^{\infty, 4} \psi_{n,l,q}^\dagger \right) |0\rangle. \quad (32)$$

$|0\rangle$ is the empty state defined by $\psi_{n,l,q}|0\rangle = 0$. We are using the Dirac theory as an effective model of the underlying lattice model. The lattice model sets an ultraviolet cut-off which is proportional to the inverse of the lattice constant. We estimate a cut-off for the Landau level index by equating the number of states of the lattice model to that of the continuum model,

$$N_c = \frac{2\pi}{\sqrt{3}} \left(\frac{\ell_c}{a} \right)^2. \quad (33)$$

This amounts to replacing the detailed band structure of the lattice model with energy levels of the Dirac particle, which is an approximation in our model calculation.

We now discuss the transformation properties of the Dirac sea, i.e. the fully occupied quartet of the Landau level with $n \leq -1$. It is useful to write,

$$\psi_{n,l,q}^\dagger = \left(\int_{\mathbf{x}} \Psi_{r,A}^\dagger(\mathbf{x}) \phi_r^{n,l,q}(\mathbf{x}) \right) \chi_A^q \equiv \tilde{\psi}_{n,l,q,A}^\dagger \chi_A^q \quad (34)$$

Now consider the product of the operators that create the quartet at every occupied n, l ,

$$\tilde{\psi}_{n,l,1,A_1}^\dagger \tilde{\psi}_{n,l,2,A_2}^\dagger \tilde{\psi}_{n,l,3,A_3}^\dagger \tilde{\psi}_{n,l,4,A_4}^\dagger \chi_{A_1}^1 \chi_{A_2}^2 \chi_{A_3}^3 \chi_{A_4}^4 \quad (35)$$

If all the eigenvalues, m_q , are equal, then $\tilde{\psi}_{n,l,q,A}^\dagger$ is independent of q . In such a case the product of the $\tilde{\psi}$ operators is proportional to the totally antisymmetric tensor $\epsilon_{A_1, A_2, A_3, A_4}$. Since the matrix formed by the eigenvectors, χ_A^q , is a unitary matrix, the χ^q dependence of the product in Eq.(35) is just a phase and thus the state is invariant under $U(4)$ (and hence $SU(4)$) transformations.

However, if all the m_q are not equal to each other, then the product is not invariant under all the $U(4)$ transformations. The subgroup, \mathcal{G} , under which the product is invariant (up to a phase) is the set of $U(4)$ matrices that commute with the diagonal matrix, $M_D = \{m_1, m_2, m_3, m_4\}$. The ground state manifold is then the coset space $U(4)/\mathcal{G}$. The smallest \mathcal{G} is $U(1) \times U(1) \times U(1) \times U(1)$, which is the case where all the four eigenvalues, m_q , are unequal. The dimension of the coset space is then 12.

Thus, our choice of the variational wave function with the mass matrix as the variational parameter allows us to have an $SU(4)$ polarization both for a partially filled $n = 0$ Landau level quartet and the filled Dirac sea. Several patterns of symmetry breaking are possible in our ansatz. The specific values taken by the variational parameters (the elements for the mass matrix, M) and the symmetry breaking pattern will be fixed by the minimization of the variational ground state energy.

V. CORRELATION FUNCTION

The computation of the variational energy requires the evaluation of the expectation value of the two point field operators. This results from a Wick decomposition applied to the four fermion terms in the interacting model. We define a two-point correlation function,

$$\Gamma_{r,A;s,B}(\mathbf{x}, \mathbf{y}) = \frac{1}{2} \langle GS | [\Psi_{s,B}^\dagger(\mathbf{y}), \Psi_{r,A}(\mathbf{x})] | GS \rangle. \quad (36)$$

$|GS\rangle$ is the ground state under consideration. Expressing the two point correlation function in terms of wavefunctions of massive Dirac particles,

$$\Gamma(\mathbf{x}, \mathbf{y}) = \sum_{q=1}^4 G_{m_q}(\mathbf{x}, \mathbf{y}) P_q. \quad (37)$$

$P_q \equiv \chi^q (\chi^q)^\dagger$, are the projection operators constructed from the eigenvectors of M . $G_{m_q}(\mathbf{x}, \mathbf{y})$ is the equal time Feynman propagator for a $(2+1)d$ massive Dirac particle with mass m_q in a magnetic field (Details in Appendix A),

$$G_{m_q}(\mathbf{x}, \mathbf{y}) = \frac{1}{2} \sum_{\substack{n=-\infty, \\ l=-|n|}}^{\infty, \infty} \left(\Theta(-\epsilon_{n,l,q}) - \Theta(\epsilon_{n,l,q}) \right) \phi^{n,l,q}(\mathbf{x}) (\phi^{n,l,q}(\mathbf{y}))^\dagger.$$

$\Theta(x)$ is the Heaviside step function and $\epsilon_{n,l,q}$ are the eigenvalues for Landau levels for the massive Dirac particle, Eq.(A2). $G_{m_q}(\mathbf{x}, \mathbf{y})$ can be expressed in the so called ‘heat kernel’ representation.

$$G_{m_q}(\mathbf{x}, \mathbf{y}) = -\frac{1}{2\sqrt{\pi}} \int_{\frac{1}{2N_C}}^{\infty} \langle \mathbf{x} | h_{m_q} e^{-s h_{m_q}^2} | \mathbf{y} \rangle. \quad (38)$$

Here, $h_{m_q} = \boldsymbol{\alpha} \cdot \boldsymbol{\pi} + \beta m_q$, is the one-particle hamiltonian for a Dirac particle with mass m_q in a magnetic field. We make use of the imaginary time propagator for a non-relativistic $2d$ electron in a magnetic field to evaluate¹⁸

$$\langle \mathbf{x} | e^{-s h_{m_q}^2} | \mathbf{y} \rangle = \frac{1}{2\pi} \zeta_s(\mathbf{x}, \mathbf{y}) \frac{e^{-s m_q^2}}{2 \sinh(s)} \begin{pmatrix} e^{-s} & 0 \\ 0 & e^s \end{pmatrix}. \quad (39)$$

Here, $\zeta_s(\mathbf{x}, \mathbf{y}) = e^{-\frac{1}{4}|\mathbf{x}-\mathbf{y}|^2 \coth(s)} e^{\frac{i}{2}(x_1 y_2 - y_1 x_2)}$.

By construction, $\Gamma(\mathbf{x}, \mathbf{y})$ is an 8×8 matrix. The mass matrix, M , for the Dirac particles of graphene encodes the information about the filling factor and the nature of the ground state,

$$M = \sum_{q=1}^4 m_q P_q. \quad (40)$$

We fix the chemical potential at zero for all the calculations discussed in this article. The signs of m_q then decide which members of the quartet of the $n = 0$ Landau level are occupied. With our convention, the q^{th} member is occupied if m_q is positive. Hence, for $\sigma_H = 0$, the diagonal mass matrix takes the form $M_D = \{m_1, m_2, -m_3, -m_4\}$, with $m_q > 0$ for $q = 1, \dots, 4$. Similarly, $M_D = \{m_1, -m_2, -m_3, -m_4\}$ for $\sigma_H = -1$.

The two point correlator, Eq.(37), enables us to compute the energy of the long-ranged Coulomb interaction efficiently. It eliminates the need to compute the matrix elements of individual wavefunctions and the computation reduces to the evaluation of a few well behaved two dimensional integrals.

The mean field energy computation for the symmetric breaking terms of the interacting model is expressed in terms of the coincident correlator, which is independent of spatial coordinates, $\Gamma = \sum_{q=1}^4 G_{m_q}(\mathbf{x}, \mathbf{x}) P_q$,

$$\Gamma = \frac{1}{2\pi} \sum_{q=1}^4 \frac{1}{2} (u_{m_q} \mathbb{1}_2 - v_{m_q} \beta) \otimes P_q. \quad (41)$$

Here, u_{m_q} and v_{m_q} are evaluated using the following integrals,

$$u_{m_q} = \frac{m_q}{2\sqrt{\pi}} \int_{\frac{1}{2N_C}}^{\infty} \frac{ds}{\sqrt{s}} e^{-s m_q^2}. \quad (42)$$

$$v_{m_q} = \frac{m_q}{2\sqrt{\pi}} \int_{\frac{1}{2N_C}}^{\infty} \frac{ds}{\sqrt{s}} e^{-s m_q^2} \coth(s). \quad (43)$$

In the limit of a large cut-off we have $\lim_{N_C \rightarrow \infty} u_m \rightarrow \text{sgn}(m_q)/2$. For the magnetic field values relevant to us, u_m is very close to $1/2$. Specifically, $0 \leq (0.5 - |u_{m_q}|) \leq 0.001$. This small deviation from 0.5 is due to our cut-off procedure. Henceforth we will put $u_{m_q} = 0.5 \text{sgn}(m_q)$. Since $\coth(s) \geq 1$, we always have $|v_{m_q}| \geq 0.5$.

The two point correlators, Eq.(37), and the two point coincident correlators, Eq.(41), will be used to evaluate the variational state energy for the interacting model in the following sections.

VI. SEA POLARIZATION

In section IV, we had shown that the filled Dirac sea of Landau levels ($n = -N_C, \dots, -1$), in general, is not an $SU(4)$ singlet when the parameters m_q are unequal. In this section we characterize this symmetry breaking in terms of the order parameters defined in section III B.

We can use the expression for the coincident correlation function in Eq.(41) to evaluate the order parameters,

$$\langle \mathcal{T}^{\mu\nu}(\mathbf{x}) \rangle = \text{Tr}[(\mathbb{1}_2 \otimes T^{\mu\nu})\Gamma]. \quad (44)$$

$$\langle \tilde{\mathcal{T}}^{\mu\nu}(\mathbf{x}) \rangle = \text{Tr}[(\beta \otimes T^{\mu\nu})\Gamma]. \quad (45)$$

The contribution from the Dirac sea can be obtained by deducting the $n = 0$ Landau level contributions from the above equations. Denoting the sea contribution to the order parameters by $\langle \dots \rangle_{sea}$, this gives us,

$$\langle \mathcal{T}^{\mu\nu}(\mathbf{x}) \rangle_{sea} = \frac{1}{2\pi} \sum_{q=1}^4 \left(u_{m_q} - \frac{\text{sgn}(m_q)}{2} \right) \text{Tr}[T^{\mu\nu} P_q]. \quad (46)$$

$$\langle \tilde{\mathcal{T}}^{\mu\nu}(\mathbf{x}) \rangle_{sea} = -\frac{1}{2\pi} \sum_{q=1}^4 \left(v_{m_q} - \frac{\text{sgn}(m_q)}{2} \right) \text{Tr}[T^{\mu\nu} P_q]. \quad (47)$$

Since $u_{m_q} = 0.5 \text{sgn}(m_q)$, we have $\langle \mathcal{T}^{\mu\nu}(\mathbf{x}) \rangle_{sea} = 0$. Since $|v_{m_q}| > 0.5$, the staggered polarization of the sea is, in general, non-zero.

Thus the Dirac sea of our variational states breaks the $SU(4)$ symmetry by developing a staggered polarization. However, the net $SU(4)$ polarization for the Dirac sea is zero. To visualize this, consider the non-interacting ground state. This corresponds to $m_q = 0$ and the sea is a singlet which has all the charges uniformly distributed over the lattice sites. Now consider making one of the m_q non-zero. The wave function of this species will have different weights on the two sublattices with the total weight in a unit cell remaining unchanged. Thus the sea will develop a staggered polarization but not a net polarization.

VII. SYMMETRIC MODEL

In this section, we consider the leading order (in a/ℓ_c) part of the hamiltonian which includes the kinetic term, Eq.(5), and the Coulomb term, Eq.(14).

$$\mathcal{H}_0 = \mathcal{H}_t + \mathcal{H}_C. \quad (48)$$

Both these terms are $SU(4)$ symmetric. The charge densities that occur in \mathcal{H}_C are with respect to the average charge density at half filling.

We will evaluate the variational state energy of \mathcal{H}_0 , minimize it, and show that the $SU(4)$ symmetry is spontaneously broken down to $U(1) \times SU(3)$ for $\sigma_H = -1$ and $SU(2) \times SU(2)$ for $\sigma_H = 0$. We also compute the gaps of the quasi-particle(hole) excitations within the symmetric model.

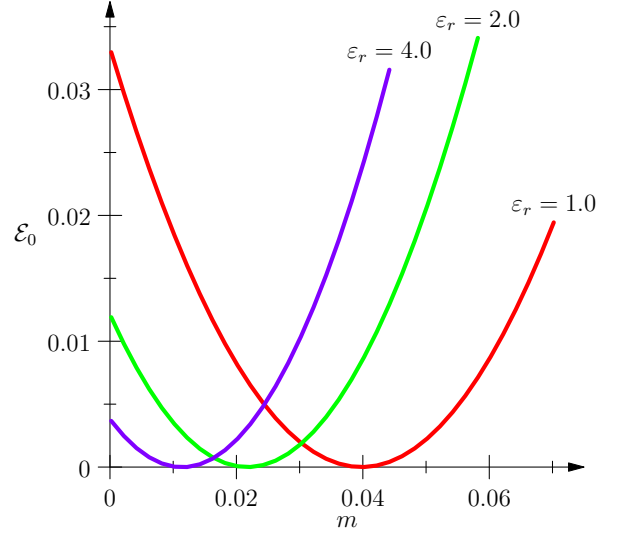


FIG. 1. This figure shows the ground state energy density as a function of the variational parameter m for $\varepsilon_r = 1, 2, 4$. The minima of the energy density function decreases with increasing ε_r . The curves have been adjusted to align the minima along the m -axis.

A. Ground states

In this subsection, we use the two point correlator, Eq.(37), to compute the expectation value of the kinetic and the Coulomb terms. The evaluation of these expectation values involves the integration of the s variables of the correlators, Eq.(38), which is accomplished numerically.

The kinetic term has local fermion field operators and the expectation value can be expressed as,

$$\langle \mathcal{H}_t \rangle = \kappa_t \int_{\mathbf{x}} \lim_{\mathbf{y} \rightarrow \mathbf{x}} \langle \Psi_{r,A}^\dagger(\mathbf{x}) \langle \mathbf{x} | \mathbf{h}_{r,A;s,B} | \mathbf{y} \rangle \Psi_{s,B}(\mathbf{y}) \rangle. \quad (49)$$

Here $\mathbf{h}_{r,A;s,B} = (\boldsymbol{\alpha} \cdot \boldsymbol{\pi})_{r,s} (\mathbb{1}_4)_{A,B}$, Eq.(5). Using the two point correlator, Eq.(37), the kinetic energy density, $\mathcal{E}_t \equiv \langle \mathcal{H}_t \rangle$, of the variational state is evaluated to give

$$\mathcal{E}_t = \frac{\kappa_t}{2\pi} \sum_{q=1}^4 \eta_t(m_q^2). \quad (50)$$

Here the quantity η_t depends on the square of the mass parameter and is a positive quantity which we evaluate numerically (Details in Appendix B 1).

The expectation value of the Coulomb term, Eq.(14), can be expressed in terms of the two point correlator,

$$\langle \mathcal{H}_C \rangle = -\kappa_C \iint_{\mathbf{x}, \mathbf{y}} \frac{1}{|\mathbf{x} - \mathbf{y}|} \text{Tr}[\Gamma(\mathbf{x}, \mathbf{y}) \Gamma(\mathbf{y}, \mathbf{x})].$$

The Coulomb energy density, $\mathcal{E}_C \equiv \langle \mathcal{H}_C \rangle$, is evaluated

using the two-point correlators,

$$\mathcal{E}_C = -\frac{\kappa_C}{2\pi} \sum_{q=1}^4 \eta_{C_2}(m_q^2). \quad (51)$$

The quantity η_{C_2} also depends on the square of the mass parameter and its numerical evaluation involves double integration of the variable s of the correlator (Details in Appendix B 2).

The total energy of the leading order hamiltonian, \mathcal{H}_0 , is therefore a sum of functions of m_q^2 ,

$$\mathcal{E}_0 = \mathcal{E}_t + \mathcal{E}_C = \sum_{q=1}^4 \left(\kappa_t \eta_t(m_q^2) - \kappa_C \eta_{C_2}(m_q^2) \right). \quad (52)$$

Thus the energy minimization condition, $\partial \mathcal{E}_0 / \partial m_q = 0$, implies that the magnitudes of all the masses, m_q , are equal. Fig.1 shows the energy as a function of m_q . The minimum of energy density at a non-zero value of m_q decreases with an increasing dielectric constant (decreasing interaction strength).

The filling factor (Hall conductivity) determines the signs of the masses. For $\sigma_H = -1$, three of the masses are negative and one positive. For $\sigma_H = 0$, two are positive and two negative. The non-zero values of m_q imply that the $SU(4)$ symmetry is spontaneously broken. As we discuss below, the signs of the masses determine the patterns of the symmetry breaking for the two cases.

1. Ground state at manifold $\sigma_H = -1$

The many body ground state at $\sigma_H = -1$ has a quarter-filled quartet of the $n = 0$ Landau level. Thus after minimization, the diagonal mass matrix for the ground state at $\sigma_H = -1$ takes the form,

$$M_D = \{m, -m, -m, -m\}. \quad (53)$$

The ground state at Hall conductivity $\sigma_H = -1$ is therefore invariant under a subgroup, $U(1) \times U(3)$, of $U(4)$. The ground state manifold is a coset space $U(4)/(U(1) \times U(3)) = CP^3$. The dimension of this coset space is six and is completely specified by a normalized four component complex vector (up to a phase). This complex vector corresponds to the $SU(4)$ component of the wavefunction of the occupied member of the $n = 0$ Landau level quartet. Without loss of generality, we choose the $SU(4)$ component to be χ^1 and parameterize it as,

$$|\chi^1\rangle = \cos(\frac{\gamma_1}{2})|+\rangle|\mathbf{n}_1\rangle + e^{i\Omega_1} \sin(\frac{\gamma_1}{2})|-\rangle|\mathbf{n}_2\rangle. \quad (54)$$

Here $|\pm\rangle|\mathbf{n}_i\rangle \equiv |\pm\rangle \otimes |\mathbf{n}_i\rangle$. And $|\pm\rangle$ are the eigenvectors of the valley operator τ^z . $|\mathbf{n}_i\rangle$ is a vector pointing in an arbitrary direction in the spin space.

$$|\mathbf{n}_i\rangle = \cos(\frac{\theta_i}{2})|\uparrow\rangle + e^{i\varphi_i} \sin(\frac{\theta_i}{2})|\downarrow\rangle. \quad (55)$$

Here $|\uparrow\rangle$ and $|\downarrow\rangle$ are the eigenvectors of σ^z .

The mass matrix for the ground state at $\sigma_H = -1$ is

$$M = m \left(2|\chi^1\rangle\langle\chi^1| - \mathbb{1}_4 \right) \equiv mQ^{(-1)}, \quad (56)$$

where $Q^{(-1)}(\gamma_1, \Omega_1, \theta_1, \phi_1, \theta_2, \phi_2)$ is a 4×4 matrix valued function of the six angle parameters. It is in one-to-one correspondence with the elements of the coset space $U(4)/(U(3) \times U(1))$. It satisfies the properties, $(Q^{(-1)})^2 = \mathbb{1}_4$ and $\text{Tr}[Q^{(-1)}] = -2$.

The mass parameter m and Q , which is parameterized by the six angle parameters, make it seven variational parameters to describe the degenerate ground states of \mathcal{H}_0 at $\sigma_H = -1$.

2. Ground state manifold at $\sigma_H = 0$

For the ground state at $\sigma_H = 0$, the diagonal mass matrix is,

$$M_D = \{m, m, -m, -m\}. \quad (57)$$

The manifold for the ground state in this case is a coset space $U(4)/(U(2) \times U(2))$. The dimension of this coset space is eight.

For this case, we need to construct two four component vectors that specify the $SU(4)$ components of the two occupied members of the $n = 0$ Landau level quartet. Eq.(54) describes the first vector. The second vector is orthonormal to Eq.(54) and can be constructed explicitly, requiring two more angle parameters,

$$|\chi^2\rangle = \cos(\frac{\gamma_2}{2})|+\rangle|\mathbf{n}_1\rangle + e^{i\Omega_2} \sin(\frac{\gamma_2}{2})|-\rangle|\mathbf{n}_2\rangle. \quad (58)$$

The mass matrix is of the form,

$$M = m \left(2(|\chi^1\rangle\langle\chi^1| + |\chi^2\rangle\langle\chi^2|) - \mathbb{1}_4 \right) \equiv mQ^{(0)}, \quad (59)$$

where $Q^{(0)}(\gamma_1, \Omega_1, \gamma_2, \Omega_2, \theta_1, \phi_1, \theta_2, \phi_2)$ is a 4×4 matrix valued function of the eight angle parameters. It is in one-to-one correspondence with the elements of the coset space $U(4)/(U(2) \times U(2))$. It satisfies the properties, $(Q^{(0)})^2 = \mathbb{1}_4$ and $\text{Tr}[Q^{(0)}] = 0$.

The mass parameter m and Q , which is parameterized by the eight angle parameters, make it nine variational parameters to describe the degenerate ground states of \mathcal{H}_0 at $\sigma_H = 0$.

B. Excitation states and gaps

In this subsection we will compute the activation gaps for \mathcal{H}_0 , which is the excitation energy of a well separated quasi-particle and quasi-hole pair. In our case, the excited states at Hall conductivity, $\sigma_H = 0, -1$, the particle

and the hole quantum numbers belong to different members of the $n = 0$ Landau level quartet. The excited state is defined as,

$$|ES\rangle = \psi_{0,l_p,q_p}^\dagger \psi_{0,l_h,q_h} |GS\rangle. \quad (60)$$

The activation gap is evaluated from the expectation value of the hamiltonian for the excited state and for the ground state, defined as the following,

$$\Delta_{gap} = \frac{1}{2} (\langle ES | \mathcal{H} | ES \rangle - \langle GS | \mathcal{H} | GS \rangle). \quad (61)$$

The ground state expectation value of the hamiltonian is expressed in terms of two point correlators, used for variational state energy calculation. In a similar fashion, we can define the two point correlator for excited states, $\Upsilon(\mathbf{r}_1, \mathbf{r}_2)$ as,

$$\Upsilon_{r,A;s,B}(\mathbf{r}_1, \mathbf{r}_2) = \langle ES | \Psi_{s,B}^\dagger(\mathbf{r}_2) \Psi_{r,A}(\mathbf{r}_1) | ES \rangle. \quad (62)$$

This correlator is an 8×8 matrix and can be expressed as following,

$$\Upsilon(\mathbf{r}_1, \mathbf{r}_2) = \Gamma^{(p)}(\mathbf{r}_1, \mathbf{r}_2) - \Gamma^{(h)}(\mathbf{r}_1, \mathbf{r}_2) + \Gamma(\mathbf{r}_1, \mathbf{r}_2). \quad (63)$$

Here $\Gamma^{(p)}(\mathbf{r}_1, \mathbf{r}_2)$ and $\Gamma^{(h)}(\mathbf{r}_1, \mathbf{r}_2)$ are the two point correlators for the particle and the hole states respectively and $\Gamma(\mathbf{r}_1, \mathbf{r}_2)$ is the two point correlator for the ground state.

The correlator for the particle or hole, ($\mathbf{x} = p, h$)

$$\begin{aligned} \Gamma^{(\mathbf{x})}(\mathbf{r}_1, \mathbf{r}_2) &= \Phi^{0,l_x,q_x}(\mathbf{r}_1) \Phi^{0,l_x,q_x^\dagger}(\mathbf{r}_2) \\ &= \frac{1}{4\pi} (1 - \beta) \frac{1}{l_x!} \left(\frac{\bar{z}_1 z_2}{2} \right)^{l_x} \\ &\quad e^{-\frac{1}{4}(\bar{z}_1 z_2 + z_1 \bar{z}_2)} e^{-\frac{1}{4}|z_1 - z_2|^2} P_{q_x}. \end{aligned} \quad (64)$$

Within the symmetric model ($\mathcal{H} = \mathcal{H}_0$ in Eq.(61)), we will show that the $SU(4)$ component of the correlator gets traced out and there is no angle dependence for the activation gaps. Moreover, we consider the case where the particle and the hole are separated by a large distance, hence excluding the possibility of particle-hole bound states.

The contribution to the activation gap from the kinetic term is evaluated as,

$$\begin{aligned} \Delta_t &= \frac{\kappa_t}{2} \left(\int_{\mathbf{r}} \lim_{\mathbf{r}_0 \rightarrow \mathbf{r}} \text{Tr}[\mathbf{h} \Upsilon(\mathbf{r}, \mathbf{r}_0)] \right. \\ &\quad \left. - \int_{\mathbf{r}} \lim_{\mathbf{r}_0 \rightarrow \mathbf{r}} \text{Tr}[\mathbf{h} \Gamma(\mathbf{r}, \mathbf{r}_0)] \right). \end{aligned} \quad (65)$$

We find no contribution to the activation gap from the kinetic term. This is not surprising because of the fact that the $n = 0$ Landau level wavefunctions are the same for both the massless and the massive Dirac particle. And the massless Dirac particle has zero eigenvalue for the $n = 0$ Landau level.

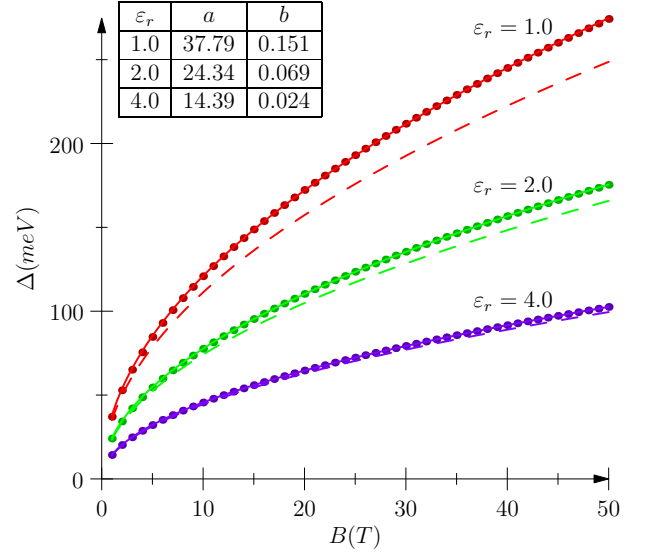


FIG. 2. This figure shows the variation of activation gap with magnetic field. The gaps for the Hall conductivity at $\sigma_H = 0$ and $\sigma_H = -1$ are same. The solid points are values for the gap obtained from our calculations. The solid line shows the best fit for the gaps as function of magnetic field of the form $a\sqrt{B} + bB$. a, b are best fit parameters shown in the inset for three dielectric constants. We have shown the variation of gaps with change in the dielectric constant of the substrate. The dielectric constant $\varepsilon_r = 1$ corresponds to the suspended graphene. The best fit showed the dominant \sqrt{B} contribution and linear B decreases as the dielectric constant of substrate increased. The dashed lines shows the gaps when the effects of the filled Dirac sea are ignored.

The large distance separating the particle and hole results in Coulomb term contributions to the activation gap which is given by,

$$\begin{aligned} \Delta_C &= \kappa_C \iint_{\mathbf{r}_1, \mathbf{r}_2} \frac{1}{|\mathbf{r}_1 - \mathbf{r}_2|} \left(\text{Tr}[\Gamma^{(h)}(\mathbf{r}_1, \mathbf{r}_2) \Gamma(\mathbf{r}_2, \mathbf{r}_1)] \right. \\ &\quad \left. - \text{Tr}[\Gamma^{(p)}(\mathbf{r}_1, \mathbf{r}_2) \Gamma(\mathbf{r}_2, \mathbf{r}_1)] \right). \end{aligned} \quad (66)$$

The gaps turn out to be the same for both the cases, $\sigma_H = 0$ and $\sigma_H = -1$. The ground state correlators are specified by their respective mass matrix and we also use the fact from energy minimization, $m_h = m = -m_p$.

The activation gap within the symmetric model for the Hall conductivity at $\sigma_H = 0, -1$, is

$$\Delta_{gap} = \kappa_C \eta_{C_1}(m). \quad (67)$$

The coefficient $\eta_{C_1}(m)$ is evaluated numerically,

$$\eta_{C_1} = \frac{m}{2} \int_{\frac{1}{2N_C}}^{\infty} ds \frac{e^{-m^2(s-\frac{1}{2})}}{\sqrt{s \sinh(s)}}. \quad (68)$$

The variation of the particle-hole gap with the magnetic field is shown in Fig.2. We observe that the gaps have

dominant \sqrt{B} contribution and a few percent contribution from the linear term.

We have compared the results of our analysis with the case when the effects of the filled Dirac sea are ignored. In Fig.2, we have also presented the variation of gaps with dielectric constant of the substrate. At low magnetic fields, there is negligible contribution from the filled Dirac sea. Gaps shows systematic decrease in the contribution from the filled Dirac sea with the increase of dielectric constant.

VIII. SYMMETRY BREAKING TERMS

In this section, we investigate the effects of the symmetry breaking terms of our interacting model, Eq.(20), on the ground state and excitations at $\sigma_H = 0, -1$. The symmetry breaking terms are a factor of a/ℓ_c smaller when compared with the $SU(4)$ symmetric terms. Hence, a change to the minimum value of the mass parameters obtained from the symmetric model analysis will be smaller by a factor of a/ℓ_c . The range of parameter (U and V) values of our interest and $a/\ell_c \ll 1$, allow us to conclude that the effect of the symmetry breaking terms on the minimum value of the mass parameter is negligibly small. We fix the mass parameter values from the symmetric model analysis, Eq.(59) and Eq.(56) at $\sigma_H = 0, -1$ respectively. This amounts to treating the symmetry breaking terms as perturbations about the symmetric model solutions.

The variational state energy can be expressed in terms of various traces of the coincident correlator, Eq.(41), which takes the form,

$$\Gamma = \frac{1}{4\pi}(u_m \mathbb{1}_2 - v_m \beta) \otimes Q^{(\sigma_H)}. \quad (69)$$

Here $Q^{(\sigma_H)}$ are 4×4 matrices specified at $\sigma_H = 0, -1$ discussed in Sec.VII A 2 and Sec.VII A 1.

$$Q^{(\sigma_H)} = \sum_{j \in \text{occ}} P_j - \sum_{j \in \text{unocc}} P_j = 2 \sum_{j \in \text{occ}} P_j - \mathbb{1}_4, \quad (70)$$

is constructed from the $SU(4)$ components of the occupied members of the $n = 0$ Landau level quartet. The coincident correlator is position independent, the spatial integration is trivial and results in volume of the system. We derive the general expression for the expectation value of symmetry breaking terms in terms of various traces of the coincident correlator and then apply to the specific cases of $\sigma_H = 0$ and $\sigma_H = -1$.

The variational energy density for the nearest neighbour term, $\mathcal{E}_V \equiv \langle \mathcal{H}_V \rangle$, is expressed in terms of the traces of the coincident correlator as following,

$$\mathcal{E}_V = \frac{\kappa_V}{4\pi^2} \left(-\text{Tr}[\Gamma \Gamma] - (\text{Tr}[\beta \tau^z \Gamma])^2 + \text{Tr}[\beta \tau^z \Gamma \beta \tau^z \Gamma] \right). \quad (71)$$

Similarly, $\mathcal{E}_U \equiv \langle \mathcal{H}_U \rangle$, the variational state energy density for the Hubbard term,

$$\mathcal{E}_U = \frac{\kappa_U}{4\pi^2} \left(-\text{Tr}[\Gamma \Gamma] + (\text{Tr}[\beta \tau^z \Gamma])^2 - \text{Tr}[\beta \tau^z \Gamma \beta \tau^z \Gamma] + \frac{1}{2} \sum_{j,k=x,y} \left((\text{Tr}[\alpha^j \tau^k \Gamma])^2 - \text{Tr}[\alpha^j \tau^k \Gamma \alpha^j \tau^k \Gamma] \right) \right). \quad (72)$$

The Zeeman energy density, $\mathcal{E}_Z \equiv \langle \mathcal{H}_Z \rangle$, in terms of the coincident correlator,

$$\mathcal{E}_Z = -\frac{\kappa_Z}{2\pi} \text{Tr}[\sigma^z \Gamma]. \quad (73)$$

The expectation value of \mathcal{H}_{t_1} is obtained by a procedure similar to the one discussed in Sec.VII A for the kinetic term.

$$\langle \mathcal{H}_{t_1} \rangle = \kappa_{t_1} \int_{\mathbf{r}} \lim_{\mathbf{r} \rightarrow \mathbf{r}_0} \text{Tr}[\mathbf{h}_{t_1} \Gamma(\mathbf{r}, \mathbf{r}_0)]. \quad (74)$$

$\lim_{\mathbf{r} \rightarrow \mathbf{r}_0} \text{Tr}[\mathbf{h}_{t_1} \Gamma(\mathbf{r}, \mathbf{r}_0)] = \sum_{q=1}^4 f_1(m_q^2) \text{Tr}[\tau^z]$, here $f_1(m_q^2)$ results from the action of the off-diagonal elements of \mathbf{h}_{t_1} on $b_m(\mathbf{r}, \mathbf{r}_0)$, Eq.(A16), and $d_m(\mathbf{r}, \mathbf{r}_0)$, Eq.(A17). The trace over the $SU(4)$ indices vanishes, hence $\langle \mathcal{H}_{t_1} \rangle = 0$. Henceforth we drop the sub-leading kinetic term.

The net variational state energy, $\mathcal{E}_1 \equiv \langle \mathcal{H}_1 \rangle$, from the symmetry breaking terms,

$$\mathcal{E}_1 = \mathcal{E}_V + \mathcal{E}_U + \mathcal{E}_Z. \quad (75)$$

is numerically minimized for the angle parameters and hence determines the $SU(4)$ polarization of the variational ground state.

A. Ground states at $\sigma_H = 0$

The mass matrix for the $\sigma_H = 0$, $M_D = \{m, m, -m, -m\}$ and $Q^{(0)}$ parameterization scheme discussed in Sec.VII A 2 are included in the two point coincident correlator Eq.(69). Various traces are evaluated with this two point coincident correlator to obtain the contribution from the symmetry breaking terms as functions of the variational angle parameters.

The nearest neighbour interaction energy density,

$$\mathcal{E}_V = -\frac{\kappa_V}{4\pi^2} \left(8v_m^2 \cos(\gamma_1) \cos(\gamma_2) + 2(v_m^2 - u_m^2) (\cos^2(\gamma_1) + \cos^2(\gamma_2)) \right), \quad (76)$$

is a function of only two angle parameters γ_1 or γ_2 . Since $v_m > u_m$, the minimization of the nearest neighbour energy is solely decided by the first term in Eq.(76). It minimizes for the values $\gamma_1 = \gamma_2 = 0$ or π , which results in a charge ordered state.

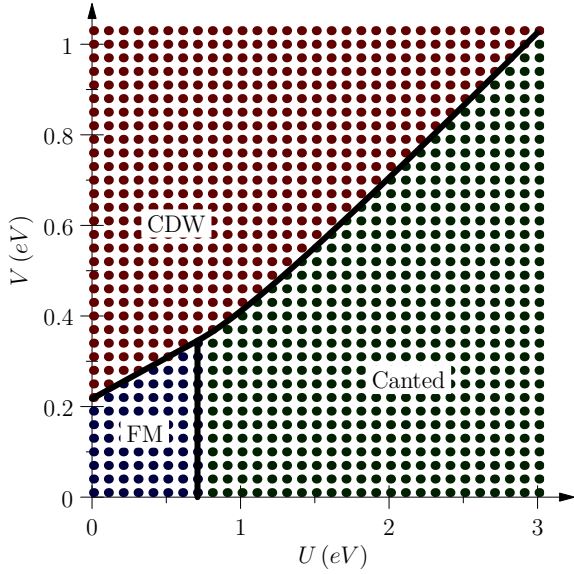


FIG. 3. The figure shows the phase diagram for possible ground states for the Hall conductivity at $\sigma_H = 0$ in U - V parameter space. This phase diagram is for the magnetic field $B = 30 T$ and $\epsilon_r = 1.0$. The region marked 'FM' is the ferromagnetic ordered state, 'CDW' is the charge ordered state and 'Canted' is the canted spin ordered state. The three regions marked with dots represents solutions obtained with numerical minimization corresponding to three phases. The bold line separating the three phases were obtained analytically after equating each pair of analytical expressions for the variational energies. Equations for these lines are given in Eq.(83), Eq.(86) and Eq.(85). Phase transition across the 'FM' and 'Canted' region is continuous whereas others are first order transition.

The variational state energy density for the Hubbard term,

$$\mathcal{E}_U = \frac{\kappa U}{4\pi^2} \left(8v_m^2 \cos(\gamma_1) \cos(\gamma_2) + 2(v_m^2 - u_m^2) (\cos(\gamma_1) - \cos(\gamma_2))^2 |\langle \mathbf{n}_1 | \mathbf{n}_2 \rangle|^2 \right), \quad (77)$$

minimizes for the values $\gamma_1 = 0$ or π , $\gamma_2 = \pi - \gamma_1$ and $|\langle \mathbf{n}_1 | \mathbf{n}_2 \rangle|^2 = 0$. These values indicate that the Hubbard term prefers a Neel ordered ground state.

The Zeeman energy contribution,

$$\mathcal{E}_Z = -\frac{\kappa Z}{2\pi} u_m (\cos(\gamma_1) - \cos(\gamma_2)) (\cos(\theta_1) + \cos(\theta_2)), \quad (78)$$

minimizes for the variational angle parameters that correspond to a ferromagnetic ordered ground state, for example: $\gamma_1 = 0$, $\gamma_2 = \pi$, $\theta_1 = 0$ and $\theta_2 = \pi$.

The angle parameters that minimize the total energy \mathcal{E}_1 for $\sigma_H = 0$ were numerically obtained. Numerical solutions correspond to three phases in the U - V parameter space shown in Fig.3 and described below.

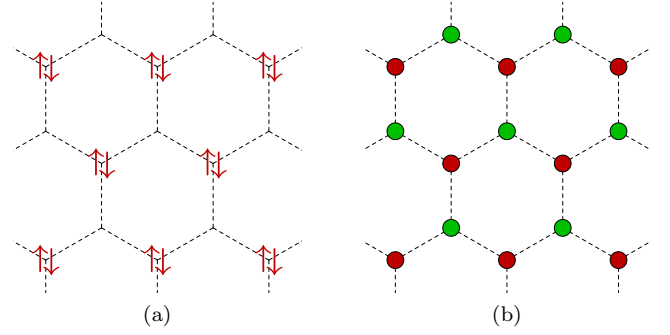


FIG. 4. One of the arrangement of $SU(4)$ components of the $n = 0$ Landau levels for the doubly degenerate charge ordered ground state shown in (a), anti-parallel spins located on same sub-lattice. The site order parameter for charge ordering shown in (b). Two colors represent the staggered charge densities on two sublattices.

1. Charge ordered state

The region marked 'CDW' shown in Fig.3 is the charge ordered ground state. The angle parameters $\gamma_1 = \gamma_2 = 0$ (or π), minimize \mathcal{E}_1 , which result in doubly degenerate ground states. This is clearly indicated by the two Q matrices, which take the form,

$$Q_{\text{CDW}}^{(0)} = \pm \tau^z \otimes \mathbb{1}_2. \quad (79)$$

The $SU(4)$ components of the two occupied quartets of the $n = 0$ Landau levels can be either $|+\rangle|\mathbf{n}\rangle$, $|+\rangle|-\mathbf{n}\rangle$ or $|-\rangle|\mathbf{n}\rangle$, $|-\rangle|-\mathbf{n}\rangle$. This results in an additional charge localized on one of the sublattice points. One of the arrangements on the graphene lattice is shown in Fig.4a. There are two order parameters for the charge ordered ground state, $\langle \mathcal{T}^{30}(\mathbf{x}) \rangle$ and $\langle \tilde{\mathcal{T}}^{30}(\mathbf{x}) \rangle$. The $SU(4)$ polarization of operator τ^z is the order parameter $\langle \mathcal{T}^{30}(\mathbf{x}) \rangle$ which results in equal bond order between the same sublattice on the graphene lattice. The staggered $SU(4)$ polarization for the τ^z operator, $\langle \tilde{\mathcal{T}}^{30}(\mathbf{x}) \rangle$ corresponds to a staggered charge distribution on the two sublattices for graphene as shown in Fig.4b. This site order parameter has dominant filled Dirac sea contributions.

2. Ferromagnetic ordered state

The region marked 'FM' for small values of U and V in Fig.3 is the ferromagnetic ordered ground state. The minimization of \mathcal{E}_1 results in the angle parameter taking values, $\gamma_1 = 0(\pi)$, $\gamma_2 = \pi(0)$, $\varphi_1 - \varphi_2 = \pi$, $\theta_1 = \theta_2 = 0(\pi)$. For these values of the angle parameters, the $SU(4)$ components of the two occupied quartet of the $n = 0$ Landau levels are $|+\rangle|\uparrow\rangle$ and $|-\rangle|\uparrow\rangle$, shown in Fig.5a. The ferromagnetic ordered state completely lifts the $SU(4)$ degeneracy and this is indicated by the Q

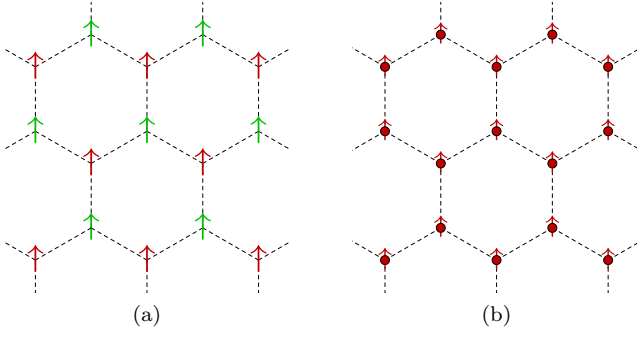


FIG. 5. The $SU(4)$ components of the $n = 0$ Landau level for the ferromagnetic ground states is shown in (a). The spin pointing along the direction of the magnetic field on each sublattice shown with different colors. The site order parameter for the ferromagnetic state, the total spin shown in (b). The small circle size indicates that this site order parameter magnitude comes from the half-filled $n = 0$ Landau level quartet.

matrix, which takes the form,

$$Q_{\text{FM}}^{(0)} = \mathbb{1}_2 \otimes \sigma^z. \quad (80)$$

The order parameters for the ferromagnetic ground state are $\langle \mathcal{T}^{03}(\mathbf{x}) \rangle$ and $\langle \tilde{\mathcal{T}}^{03}(\mathbf{x}) \rangle$. $SU(4)$ polarization of σ^z is $\langle \mathcal{T}^{03}(\mathbf{x}) \rangle$, which at lattice level corresponds to total spin polarization of the system along the direction of the magnetic field, shown in Fig.5b. The staggered $SU(4)$ polarization of σ^z is $\langle \tilde{\mathcal{T}}^{03}(\mathbf{x}) \rangle$, which at lattice level results in bond order parameters for the two sublattices with equal magnitude but opposite signs. This is analogous to the Haldane mass term¹⁷.

3. Canted-spin ordered state

The canted-spin ordered ground state in U - V parameter space is shown in Fig.3 with the region marked ‘Canted’. The angle parameters that minimize \mathcal{E}_1 are $\gamma_1 = 0(\pi)$, $\gamma_2 = \pi(0)$, $\varphi_1 - \varphi_2 = \pi$ and $\theta_1 = \theta_2 = \theta_0$, with

$$\cos(\theta_0) = +(-) \frac{1}{4} \frac{u_m}{v_m^2 - u_m^2} \frac{2\pi\kappa_Z}{\kappa_U}. \quad (81)$$

The $SU(4)$ components of the $n = 0$ Landau level for the canted ground state are $|+\rangle|\mathbf{n}_1\rangle$, $|-\rangle|\mathbf{n}_2\rangle$ and is shown in Fig.6a. $SU(4)$ degeneracy is not completely lifted, there is a remnant $U(1)$ rotation as only $\varphi_1 - \varphi_2$ is fixed by the minimization. There is a family of Q matrices for the canted ground state parameterized by the parameter φ shown below,

$$Q_{\text{Canted}}^{(0)}(\varphi) = \cos(\theta_0)\mathbb{1}_2 \otimes \sigma^z + \sin(\theta_0)\tau^z \otimes (\cos(\varphi)\sigma^x - \sin(\varphi)\sigma^y). \quad (82)$$

In general, there are six order parameters for the canted ground state, $\langle \mathcal{T}^{03}(\mathbf{x}) \rangle$, $\langle \mathcal{T}^{31}(\mathbf{x}) \rangle$, $\langle \mathcal{T}^{32}(\mathbf{x}) \rangle$,

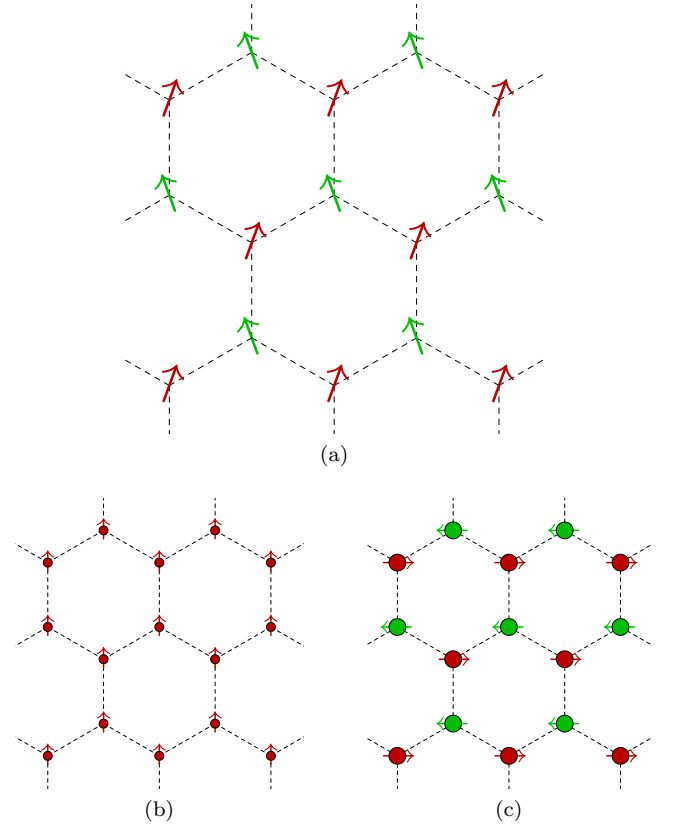


FIG. 6. The $SU(4)$ components of the $n = 0$ Landau level for the canted ground state shown in (a). The spins on sublattice shown in different colors with cant angle $2\theta_0$ between them. The site order parameter in (b), the total spin along the direction of the magnetic field on each sublattice which has contributions on from the occupied quartets of the $n = 0$ Landau levels shown with small circles. (c) shows the order parameter corresponding to Neel ordering in the direction perpendicular to the magnetic field. Larger circle size compared to order parameter in (b) is to indicate contributions from filled Dirac sea to this site order parameter.

$\langle \tilde{\mathcal{T}}^{03}(\mathbf{x}) \rangle$, $\langle \tilde{\mathcal{T}}^{31}(\mathbf{x}) \rangle$ and $\langle \tilde{\mathcal{T}}^{32}(\mathbf{x}) \rangle$. To draw the connection between these order parameters with the lattice ordering, we consider $Q_{\text{Canted}}^{(0)}$ at $\varphi = 0$. The order parameters $\langle \mathcal{T}^{03}(\mathbf{x}) \rangle$ and $\langle \tilde{\mathcal{T}}^{03}(\mathbf{x}) \rangle$ indicate ferromagnetic ordering component, described earlier in Sec.VIII A 2. The staggered order parameter for the operator $\tau^z\sigma^x$ corresponds to Neel ordering along a direction perpendicular to the magnetic field. Here in our case the Neel ordering is along the x -axis, shown in Fig.6c.

The three phases separated by bold lines shown in Fig.3, can be obtained by comparing the energies for the corresponding phases. The equation of the straight line separating the first order transition between the ferromagnetic and the charge ordered phases is given by

$$3V = \frac{1}{2} \left(1 + \frac{u_m^2}{v_m^2} \right) U + \frac{1}{4} \frac{u_m}{v_m^2} \tilde{Z}. \quad (83)$$

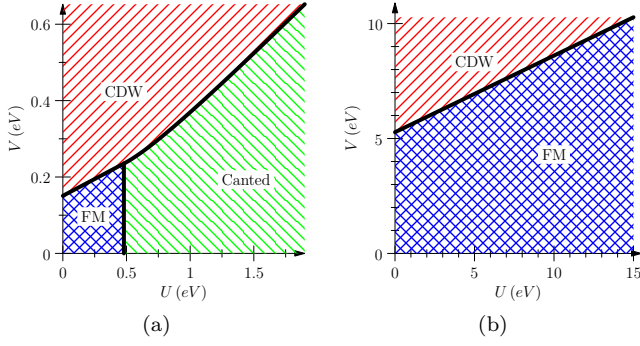


FIG. 7. (a) shows the phase diagram for $\sigma_H = 0$ at $B = 10T$ for our interacting model. (b) shows phase diagram when the effects of filled Dirac sea are ignored at any magnetic field.

Here,

$$\tilde{Z} = \frac{4\pi g\mu_B \hbar}{a^2 e^2} \frac{B_T}{B_\perp} \text{ (eV)}, \quad (84)$$

is the parameter that depends on the tilt angle and for $B_T = B_\perp$, $\tilde{Z} \approx 15.85 \text{ eV}$. The first order transition between the charge ordered and the canted spin ordered state is separated by,

$$3V = U + \frac{1}{32} \frac{u_m^2}{v_m^2(v_m^2 - u_m^2)} \frac{\tilde{Z}^2}{U}. \quad (85)$$

This equation in the large U and V limit becomes a straight line, $3V = U$.

The transition between the ferromagnetic and the canted-spin ordered state is continuous and the straight line separating them is parallel to the V -axis given by,

$$U = \frac{1}{4} \frac{u_m}{v_m^2 - u_m^2} \tilde{Z}. \quad (86)$$

We compare our results of the variational state analysis with the calculations restricted to $n = 0$ Landau level i.e. ignoring the filled Dirac sea. The filled Dirac sea contributions to the symmetry breaking terms can be easily neglected by substituting $v_m = u_m = \frac{1}{2}$ in equations: (76), (77) and (78). The minimization of this energy results in charge ordered state and ferromagnetic ordered state in U - V parameter space and the straight line separating the first order transition between the two phases is given by, $3V = U + \tilde{Z}$, shown in Fig.7b.

The inclusion of the filled Dirac sea in our variational state analysis has resulted in a canted-spin ordered state in U - V parameter space. Moreover our variational state analysis predicts all three phases for moderate values ($< 2 \text{ eV}$) for U and V in contrast to only ferromagnetic state when calculation restricted to the $n = 0$ Landau level.

B. Ground state at $\sigma_H = -1$

The diagonal mass matrix for the $\sigma_H = -1$, $M_D = \{m, -m, -m, -m\}$ and $Q^{(-1)}$ parameterization scheme

discussed in Sec. VII A 1 are included in the two point coincident correlator, Eq.(69). The variational state energy for the symmetry breaking terms is evaluated with this two point coincident correlator.

The nearest neighbour interaction energy is a function of only one angle parameter,

$$\mathcal{E}_V = -\frac{\kappa_V}{4\pi^2} \left(2(v_m^2 - u_m^2) \cos^2(\gamma_1) \right) \quad (87)$$

and this term individually minimizes for $\gamma_1 = 0$ or π , which results in a valley polarized ground state with the spin pointing in an arbitrary direction.

The expectation value for the Hubbard term,

$$\mathcal{E}_U = -\frac{\kappa_U}{4\pi^2} \left(2(v_m^2 - u_m^2) \sin^2(\gamma_1) |\langle \mathbf{n}_1 | \mathbf{n}_2 \rangle|^2 \right), \quad (88)$$

minimizes when $\gamma_1 = \pi/2$ and $|\langle \mathbf{n}_1 | \mathbf{n}_2 \rangle|^2 = 1$. This indicates that the Hubbard term prefers a Neel ordered spin ground state.

The Zeeman energy density depends on three angle variables,

$$\mathcal{E}_Z = -\frac{\kappa_Z}{2\pi} \left(u_m \left((\cos(\theta_1) - \cos(\theta_2)) + \cos(\gamma_1) (\cos(\theta_1) + \cos(\theta_2)) \right) \right) \quad (89)$$

and it minimizes for angle parameters, $\gamma_1 = 0(\pi)$, $\theta_1 = 0(\theta_2 = \pi)$. Hence the Zeeman term prefers a valley-spin polarized ground state with spins pointing along the magnetic field.

The angle parameters obtained from the numerical minimization of the variational state energy, \mathcal{E}_1 shown in Fig.8 and the solutions correspond to two phases which we have enumerated below.

1. Valley-spin polarized state

The region marked ‘VSP’ in Fig.8 is the valley-spin polarized state. The angle parameters that minimize \mathcal{E}_1 are, $\gamma_1 = 0$, $\theta_1 = 0$ or $\gamma_1 = \pi$, $\theta_2 = 0$. The $SU(4)$ components of the $n = 0$ Landau level for valley-spin polarized state are $|+\rangle|\uparrow\rangle$ or $|-\rangle|\uparrow\rangle$ and the former is shown in Fig.9a. This ground state is doubly degenerate and the Q matrices for this ground state are

$$Q_{\text{VSP}}^{(-1)} = \frac{1}{2} (\pm (\tau^z + \tau^z \sigma^z) + \sigma^z - \mathbf{1}_4) \quad (90)$$

There are eight order parameters in total. Four $SU(4)$ polarization, $\langle \mathcal{T}^{00}(\mathbf{x}) \rangle$, $\langle \mathcal{T}^{03}(\mathbf{x}) \rangle$, $\langle \mathcal{T}^{30}(\mathbf{x}) \rangle$ and $\langle \mathcal{T}^{33}(\mathbf{x}) \rangle$, and four staggered polarization, $\langle \tilde{\mathcal{T}}^{00}(\mathbf{x}) \rangle$, $\langle \tilde{\mathcal{T}}^{03}(\mathbf{x}) \rangle$, $\langle \tilde{\mathcal{T}}^{30}(\mathbf{x}) \rangle$ and $\langle \tilde{\mathcal{T}}^{33}(\mathbf{x}) \rangle$. The lattice manifestation of order parameters that are site order parameters: $\langle \mathcal{T}^{00}(\mathbf{x}) \rangle$, is the total charge density indicating that the Fermi surface is away from the half filling for $\sigma_H = -1$. $\langle \mathcal{T}^{03}(\mathbf{x}) \rangle$

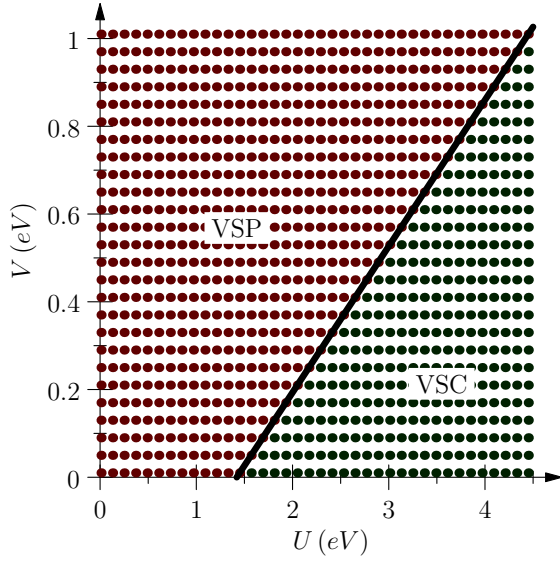


FIG. 8. The figure shows the phase diagram for the ground state at $\sigma_H = -1$ in U - V parameter space. The phase diagram shown here is for magnetic field, $B = 30$ T and $\varepsilon_r = 1.0$. The red dots mark the region ‘VSP’ corresponds to the area in parameter space where the numerical minimization yielded angle parameters for a valley-spin polarized state. The region marked ‘VSC’ corresponds where the angle parameters result in valley-spin canted state. The bold line separating the two phases is obtained by equating the energies of these two phases and equation for this line is given in Eq.(94). The order transition across this line is continuous.

is the total spin along the direction of the magnetic field, similar to what we had seen for the ferromagnetic ordered state in Sec.VIII A 2, shown in Fig.9b. $\langle \tilde{\mathcal{T}}^{30}(\mathbf{x}) \rangle$ gives the measure of the staggered charge order shown in Fig.9c. $\langle \tilde{\mathcal{T}}^{33}(\mathbf{x}) \rangle$ is the Neel ordering of the spins along the direction of the magnetic field and Fig.9d shows a caricature on graphene.

$\langle \mathcal{T}^{30}(\mathbf{x}) \rangle$ and $\langle \mathcal{T}^{33}(\mathbf{x}) \rangle$ are equal bond order parameters for both sub-lattice points. $\langle \tilde{\mathcal{T}}^{00}(\mathbf{x}) \rangle$ is the bond parameter for same sublattice points with equal magnitude and opposite sign. $\langle \tilde{\mathcal{T}}^{03}(\mathbf{x}) \rangle$ is also the bond order between same sublattice points with equal magnitude and relative sign. It also has relative sign between the spin up and spin down.

2. Valley-spin canted state:

In Fig.8, the region marked ‘VSC’ in the parameter space is where we find angle parameters that correspond to the valley-spin canted state after numerical minimization. The angle parameters take values, $\theta_1 = 0(\pi)$, $\theta_2 = \pi(0)$ and

$$\cos(\gamma_0) = +(-)\frac{1}{2}\frac{u_m}{v_m^2 - u_m^2}\frac{2\pi\kappa_Z}{\kappa_U - \kappa_V}. \quad (91)$$

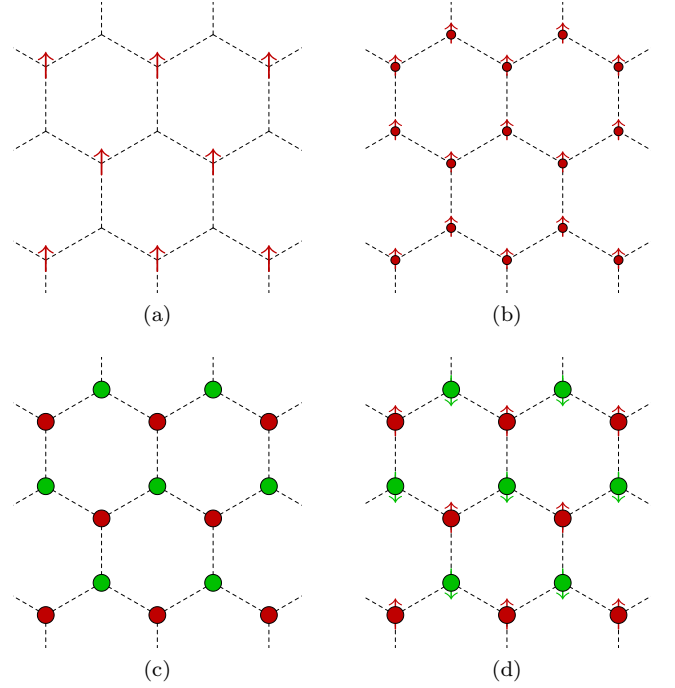


FIG. 9. (a) shows the $SU(4)$ component of $n = 0$ Landau level for one of the two degenerate ground state for valley-spin polarized ground state. (b) is the lattice manifestation of the site order parameter for the total spin along the direction of the magnetic field. (c) represents the site order parameter which is the staggered charge density on the sub-lattice points. (d) shows the Neel ordering of the spins along the direction of the magnetic field for the valley-spin polarized ground state.

The $SU(4)$ component of the occupied $n = 0$ Landau quartet,

$$|\chi^1\rangle = \cos\left(\frac{\gamma_0}{2}\right)|+\rangle|\uparrow\rangle + e^{i\Omega}\sin\left(\frac{\gamma_0}{2}\right)|-\rangle|\downarrow\rangle. \quad (92)$$

Here Ω is a free parameter. The ground state is doubly degenerate and is parameterized by one parameter, Ω , a $U(1)$ symmetry remnant of $SU(4)$. The Q matrix that characterizes the family of ground states for the valley-spin canted ground state is,

$$Q_{\text{VSC}}^{(-1)} = \frac{1}{2}\left(\pm\tau^z\sigma^z - \mathbb{1}_4 + \cos(\gamma_0)(\sigma^z \pm \tau^z) + \sin(\gamma_0)(\cos(\Omega)(\tau^x\sigma^x \mp \tau^y\sigma^y) + \sin(\Omega)(\tau^x\sigma^y \pm \tau^y\sigma^x))\right). \quad (93)$$

There are 16 order parameters for the valley-spin polarized ground state. To keep things simple, we set the parameter $\Omega = 0$ for the Q matrix, to analyze the manifestation of order parameters on the lattice. This leaves us with twelve order parameter. Eight of these parameters we have encountered in when we described the valley-spin polarized ground state. The remaining four are, $\langle \mathcal{T}^{11}(\mathbf{x}) \rangle$, $\langle \mathcal{T}^{22}(\mathbf{x}) \rangle$, $\langle \tilde{\mathcal{T}}^{11}(\mathbf{x}) \rangle$ and $\langle \tilde{\mathcal{T}}^{22}(\mathbf{x}) \rangle$. These correspond to bond order parameter between the nearest

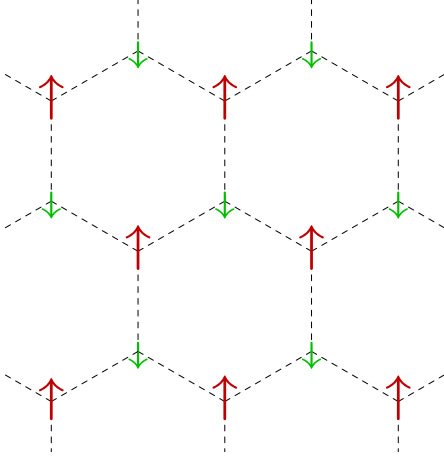


FIG. 10. The figure shows the arrangement of $SU(4)$ components of the occupied quartet of the $n = 0$ Landau level for the valley-spin canted ground state. The colors of arrows indicate spins localized on the two sub-lattice points and different lengths represents unequal weights on the sub-lattice points. The site order parameter on the lattice for the valley-spin canted ground state are same as for the valley-spin polarized ground state, shown in figures 9b, 9c and 9d.

neighbour sublattice points which also involves a momentum transfer of $\pm(\mathbf{K}_+ - \mathbf{K}_-)$.

The equation of the straight line that separates the two phases in U - V parameter space in Fig.8 is,

$$3V = U - \frac{1}{2} \frac{u_m}{v_m^2 - u_m^2} \tilde{Z}, \quad (94)$$

which we obtained by comparing the energies of the two phases. The order of the phase transition across this straight line is continuous.

Once again we compare the results of energy minimization at $\sigma_H = -1$ with the case when the effects of the filled Dirac sea are ignored. We find no contribution to the variational state energy from the symmetry breaking interaction terms. This is not surprising as $\sigma_H = -1$ has quarter-filled $n = 0$ Landau level. The only contribution comes from the Zeeman term which results in the valley-spin polarized ground state in the entire U - V parameter space. The valley-spin canted ground state is the consequence of the filled Dirac sea effects within our variational analysis.

C. Excitation states and gaps

The quasi-particle(hole) excitations from the symmetric model provided the magnitude of the gaps. The exact nature of these excitations, i.e. $SU(4)$ components of the excitations were left unspecified. In this section we compute the contributions to the particle-hole excitations from the $SU(4)$ symmetry breaking terms of our model. The ground state has been fixed in the U - V phase

space by local terms as we had seen in the previous section. The gaps from the local interaction terms are lower by a factor of (a/ℓ_c) when compared to the magnitude from long-ranged Coulomb interaction. But the angle parameter dependence that results from symmetry breaking terms will fix the $SU(4)$ components of the excitations.

To compute the contribution to the particle-hole gap from the short ranged interaction terms, we need to compute

$$\langle ES | (\Psi^\dagger(\mathbf{r}) \mathbf{G} \Psi(\mathbf{r}))^2 | ES \rangle - \langle GS | (\Psi^\dagger(\mathbf{r}) \mathbf{G} \Psi(\mathbf{r}))^2 | GS \rangle,$$

where the matrix $\mathbf{G} = \mathbb{1}_4, \beta\tau^z, \alpha^j\tau^k$ and $j, k = x, y$. A similar procedure that we followed for particle-hole excitations for symmetric model in section VII B, we define the two point coincident correlator for the excited state,

$$\Upsilon(\mathbf{r}, \mathbf{r}) = \Gamma^{(p)}(\mathbf{r}, \mathbf{r}) - \Gamma^{(h)}(\mathbf{r}, \mathbf{r}) + \Gamma(\mathbf{r}, \mathbf{r}). \quad (95)$$

$\Gamma^{(p)}$ and $\Gamma^{(h)}$ are coincident correlators for the particle and the hole state using the $n = 0$ Landau level wavefunctions. $\Gamma(\mathbf{r}, \mathbf{r})$ is the coincident correlator for the ground state and has no coordinate dependence. The correlator for the particle and the hole, Eq.(64), after the coincident limit, the coordinate integration is accomplished using gamma functions, $\Gamma^{(x)} = \int_{\mathbf{r}} \Gamma^{(x)}(\mathbf{r}) = \frac{1}{2}(\mathbb{1}_2 - \beta)P_{\mathbf{x}}$, here $\mathbf{x} = p, h$.

The particle-hole gap contribution from each of the local interaction terms for the case where the separation is large between the particle and the hole states is evaluated using the following expression,

$$\Delta_{\mathbf{G}} \propto \frac{1}{2} \left((\text{Tr}[\mathbf{G} \Gamma^{(p)}] - \text{Tr}[\mathbf{G} \Gamma^{(h)}]) \text{Tr}[\mathbf{G} \Gamma] - \text{Tr}[\mathbf{G} \Gamma^{(p)} \mathbf{G} \Gamma] + \text{Tr}[\mathbf{G} \Gamma^{(h)} \mathbf{G} \Gamma] \right). \quad (96)$$

The Zeeman term contribution to the gap is,

$$\Delta_Z = \frac{1}{2} \kappa_Z (\text{Tr}[\sigma^z \Gamma^{(p)}] - \text{Tr}[\sigma^z \Gamma^{(h)}]). \quad (97)$$

1. Excitations for ground states at $\sigma_H = 0$

We construct the quasi-hole and the quasi-particle state by taking a linear combination of the occupied and the unoccupied members of the $n = 0$ Landau level quartet respectively for each ground state at $\sigma_H = 0$. By doing this we span all possible $SU(4)$ polarizations for the quasi-particle and the quasi-hole states for each ground state in U - V parameter space.

a. Ferromagnetic ordered state: The $SU(4)$ degeneracy is completely lifted for the ferromagnetic ground state. A general hole state is a linear combination of up-spin states, $|h\rangle = |\gamma_h\rangle |\uparrow\rangle$ and particle state of down-spin states, $|p\rangle = |\gamma_p\rangle |\downarrow\rangle$. Here $|\gamma_x\rangle = \cos(\frac{\gamma_x}{2})|+\rangle + e^{i\Omega_x} \sin(\frac{\gamma_x}{2})|-\rangle$, with $\mathbf{x} = p, h$. The net gap from the symmetry breaking terms for the ferromagnetic ground

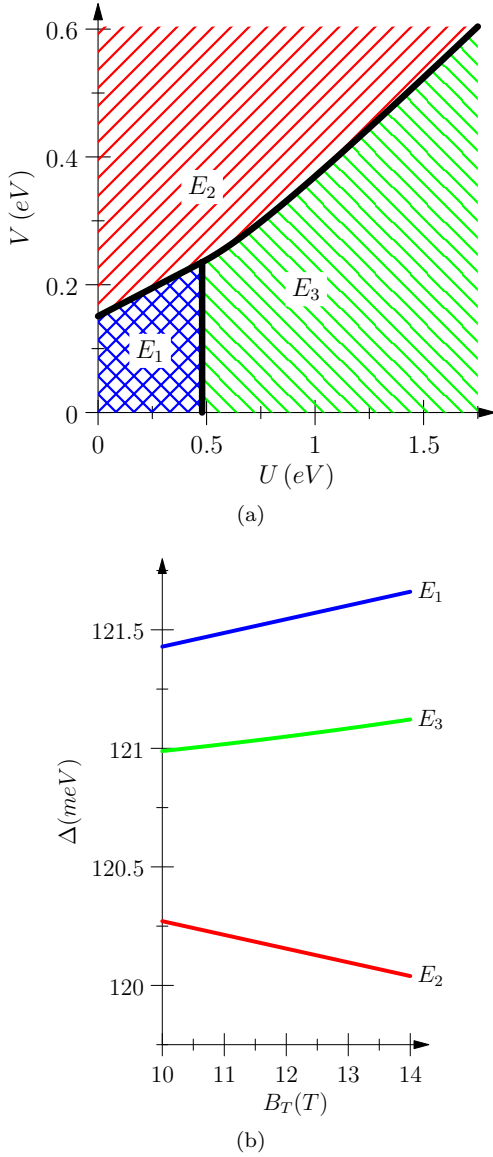


FIG. 11. (a) shows the region for all excitations from the $\sigma_H = 0$ ground state at $B_\perp = 10T$ and $\epsilon_r = 1.0$. (b) shows the variation of particle-hole gaps with respect to B_T (tilt angle $< 45^\circ$) for all the three phases for the Hall state at $\sigma_H = 0$. The gap for ferromagnetic spin ordered state labeled E_1 , increases linearly with B_T , whereas gap for the charge ordered state, labeled E_2 , decreases linearly. The gap for canted-spin phase, labeled E_3 , shows an increase with B_T with a quadratic dependence. In the canted phase, gap is inversely proportional to the Hubbard interaction strength U . In the figure we have chosen $U = 2 eV$ for the shown curve.

state is independent of angle parameters. The excitations of the ferromagnetic ground state are,

$$E_1 : |h\rangle = |\gamma_h\rangle|\uparrow\rangle, |p\rangle = |\gamma_p\rangle|\downarrow\rangle. \quad (98)$$

The quasi-particle and the quasi-holes states can be linear combinations of unoccupied and occupied members of the $n = 0$ Landau level quartet respectively. The region for the excitations, E_1 , for the ferromagnetic ground

state is marked in Fig.11a. The ferromagnetic ordered state is fully spin polarized hence the excitations will involve a spin flip, which costs a Zeeman energy, $\Delta_Z = \kappa_Z$. This brings in a linear dependence on B_T to the excitation gap shown in Fig.11b.

b. Charge ordered state: The charge ordered state is doubly degenerate as it can be localized on either valley. We choose one of them and construct the quasi-hole state by choosing a spin in an arbitrary direction localized in the valley, $|+\rangle$: $|h\rangle = |+\rangle|\mathbf{n}_h\rangle$ and $|-\rangle$ for the quasi-particle state: $|p\rangle = |-\rangle|\mathbf{n}_p\rangle$. Here the spin vector, $|\mathbf{n}_x\rangle = \cos(\frac{\theta_x}{2})|\uparrow\rangle + e^{i\varphi_x}\sin(\frac{\theta_x}{2})|\downarrow\rangle$, with $\mathbf{x} = p, h$. The only angle dependence comes from the Zeeman term, $\Delta_Z = -\frac{1}{2}\kappa_Z(\cos(\theta_p) - \cos(\theta_h))$. The net gap minimizes for $\theta_p = 0$ and $\theta_h = \pi$. The $SU(4)$ components of the excitations for the charge ordered ground state are,

$$E_2 : |h\rangle = |+\rangle|\downarrow\rangle, |p\rangle = |-\rangle|\uparrow\rangle. \quad (99)$$

The region for the excitations, E_2 , in U - V parameter space is shown in Fig.11a. The particle-hole excitations involve flipping both the valley and the spin quantum numbers and hence the lower the Zeeman energy, $\Delta_Z = -\kappa_Z$. The gap decreases linearly with B_T , shown in Fig.11b.

c. Canted spin state: For the canted spin ground state, the $SU(4)$ degeneracy is not completely lifted. We construct a family of quasi-hole states by taking a linear combination of the occupied members of the $n = 0$ Landau level quartet, $|h\rangle = \cos(\frac{\theta_h}{2})|+\rangle|\mathbf{n}_1\rangle + e^{i\varphi_h}\sin(\frac{\theta_h}{2})|-\rangle|\mathbf{n}_2\rangle$, where $\varphi_1 - \varphi_2 = \pi$ and $\theta_1 = \theta_2 = \theta_0$. The cant angle is given by the Eq.(81). A family of quasi-particle states is constructed by taking the linear superposition of unoccupied members of the $n = 0$ Landau level quartet, $|p\rangle = \cos(\frac{\theta_p}{2})|+\rangle|\mathbf{n}_1\rangle + e^{i\varphi_p}\sin(\frac{\theta_p}{2})|-\rangle|\mathbf{n}_2\rangle$. Here, like the case for the excitations of the ferromagnetic ordered ground state, the net gap from the symmetry breaking terms turns out to be independent of the angle parameters of the particle and the hole states. The excitations from the canted-spin ground state are linear combinations of the occupied and unoccupied members of the $n = 0$ Landau level quartet,

$$\begin{aligned} E_3 : |h\rangle &= \cos(\frac{\theta_h}{2})|+\rangle|\mathbf{n}_1\rangle + e^{i\varphi_h}\sin(\frac{\theta_h}{2})|-\rangle|\mathbf{n}_2\rangle \\ |p\rangle &= \cos(\frac{\theta_p}{2})|+\rangle|\mathbf{n}_1\rangle + e^{i\varphi_p}\sin(\frac{\theta_p}{2})|-\rangle|\mathbf{n}_2\rangle. \end{aligned} \quad (100)$$

The region for these excitations in U - V parameter space is shown in Fig.11a. The canted-spin state is not fully spin polarized, the excitations cost a Zeeman energy, $\Delta_Z = \kappa_Z \cos(\theta_0)$. The gaps in tilted magnetic have an increasing quadratic dependence on B_T and is shown in Fig.11b.

The tilted magnetic field measurements for the activation gaps in quantum Hall experiments are good to decipher the spin of the excitations. In tilted field experiment, B_\perp , the perpendicular component of the magnetic

field is kept fixed and B_T , the total magnetic field is varied by rotating the sample. In the Zeeman term, the spin sees only the total magnetic field. Whereas rest of the terms of our interacting model depends on the magnetic field perpendicular the plane. The particle-hole excitations from the interaction terms have a dominant contribution from the long-ranged Coulomb term and the short-ranged interactions are suppressed by a factor of a/ℓ_c , hence we ignore them in the following analysis. The dependence of total gap can be written as

$$\Delta = \Delta_C(B_\perp) + \Delta_Z(B_T). \quad (101)$$

For fixed B_\perp , the Coulomb contribution is constant, whereas the Zeeman contribution varies with B_T . The variation of gaps with B_T for the three ground states for the Hall conductivity at $\sigma_H = 0$ are shown in Fig.11b.

2. Excitations for ground states at $\sigma_H = -1$

The ground state at $\sigma_H = -1$ has quarter-filled $n = 0$ Landau level quartet and its $SU(4)$ component is used to construct the quasi-hole state. We construct a quasi-particle state by taking a linear combination of the three of the unoccupied members of the $n = 0$ Landau level quartet.

a. Valley-spin polarized state: The valley-spin polarized ground state is doubly degenerate, we choose the $SU(4)$ component for the quasi-hole state, $|h\rangle = |+\rangle|\uparrow\rangle$. The $SU(4)$ components for the quasi-particle can be constructed as the following linear combination of states,

$$|p\rangle = \cos\left(\frac{\theta_p}{2}\right)|-\rangle|\uparrow\rangle + e^{i\varphi_p} \sin\left(\frac{\theta_p}{2}\right)|\gamma_p\rangle|\downarrow\rangle. \quad (102)$$

The minimization of the net gap from the symmetry breaking terms was numerically obtained and we find three excitations for the valley-spin polarized state and they are,

$$\tilde{E}_1: \quad \theta_p = 0, \quad |p\rangle = |-\rangle|\uparrow\rangle, \quad \Delta_Z = 0. \quad (103)$$

$$\tilde{E}_2: \quad \theta_p = \pi, \gamma_p = 0, \quad |p\rangle = |+\rangle|\downarrow\rangle, \quad \Delta_Z = \kappa_Z. \quad (104)$$

$$\tilde{E}_3: \quad \theta_p = \pi, \gamma_p = \pi, \quad |p\rangle = |-\rangle|\downarrow\rangle, \quad \Delta_Z = \kappa_Z. \quad (105)$$

The region in U - V parameter space for these excitations is shown in Fig.12a. The variation of excitation gaps with B_T are shown in Fig.12b. The excitation \tilde{E}_1 has no variation with B_T whereas both \tilde{E}_2 and \tilde{E}_3 have linear and increasing dependence on B_T .

b. Valley-spin canted state: The valley-spin canted ground state is doubly degenerate and has a free parameter Ω . Here we choose the $SU(4)$ components of the quasi-hole state, $|h\rangle = \cos(\frac{\gamma_0}{2})|+\rangle|\uparrow\rangle + e^{i\Omega} \sin(\frac{\gamma_0}{2})|-\rangle|\downarrow\rangle$. γ_0 is given by Eq.(91). The $SU(4)$ components of the quasi-particle state are obtained by taking the following

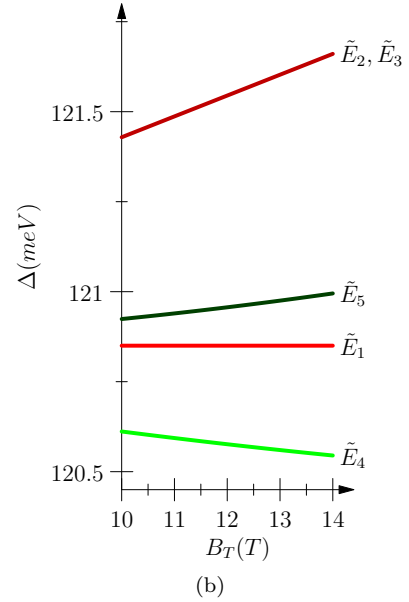
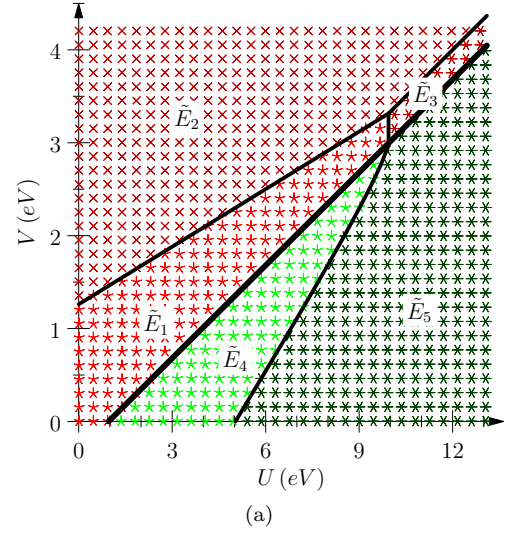


FIG. 12. The figures show the excitations described in the main text for the ground states at $\sigma_H = -1$ in the U - V parameter space, (a), and their variation with B_T (tilt angle $< 45^\circ$) in (b). The excitations \tilde{E}_1 , \tilde{E}_2 and \tilde{E}_3 are for the valley-spin polarized state and \tilde{E}_4 and \tilde{E}_5 for the valley-spin canted state. The excitations \tilde{E}_2 and \tilde{E}_3 of the valley-spin polarized state have a linear variation with B_T whereas \tilde{E}_1 has none. The excitation \tilde{E}_5 of the valley-spin canted state has a quadratic dependence on B_T whereas \tilde{E}_4 has competing increasing quadratic and decreasing linear B_T dependence. For small tilt, angles the decreasing linear B_T dependence dominate as shown in (b).

linear combination,

$$|p\rangle = \cos\left(\frac{\theta_p}{2}\right) \left(\sin\left(\frac{\gamma_0}{2}\right)|+\rangle|\uparrow\rangle - e^{i\Omega} \cos\left(\frac{\gamma_0}{2}\right)|-\rangle|\downarrow\rangle \right) + e^{i\varphi_p} \sin\left(\frac{\theta_p}{2}\right) \left(\cos\left(\frac{\gamma_p}{2}\right)|+\rangle|\downarrow\rangle + e^{i\Omega_p} \sin\left(\frac{\gamma_p}{2}\right)|-\rangle|\uparrow\rangle \right). \quad (106)$$

Minimization of the net gap from the symmetry breaking terms with respect to the variational angle parameters was performed numerically and we find two possible excitations enumerated below,

$$\begin{aligned} \tilde{E}_5 : \theta_p = 0, |p\rangle = \sin(\frac{\gamma_0}{2})|+\rangle|\uparrow\rangle - e^{i\Omega} \cos(\frac{\gamma_0}{2})|-\rangle|\downarrow\rangle, \\ \Delta_Z = \kappa_Z \cos(\gamma_0). \end{aligned} \quad (107)$$

$$\begin{aligned} \tilde{E}_4 : \theta_p = \pi, \gamma_p = \pi, |p\rangle = |+\rangle|\uparrow\rangle, \\ \Delta_Z = -\frac{1}{2}\kappa_Z(1 - \cos(\gamma_0)). \end{aligned} \quad (108)$$

The regions for these two excitations are marked \tilde{E}_4 and \tilde{E}_5 , in U - V parameter space shown in Fig.12a. The excitation \tilde{E}_5 has quadratic dependence on B_T as shown in Fig.12b. The excitation, \tilde{E}_4 , has a decreasing linear and a increasing quadratic dependence on B_T which compete with each other. At low tilt angles the decreasing linear B_T dependence dominates as shown in Fig.12b.

IX. COMPARISON WITH EXPERIMENTS

In this section, we compare the behaviour of gaps w.r.t. B_\perp and B_T with experiments^{5,14}. This analysis will demarcate a region in U - V parameter space where our model results are consistent with experiments.

In the reference [14], it was reported that the gap at $\sigma_H = 0$ for suspended graphene was good fit to $\Delta_{\sigma_H=0} = (23.1\sqrt{B} - 11.1)meV$. In Sec.VII B, we had evaluated the quasi-particle(hole) gap at $\sigma_H = 0$ and found that it was a good fit to, $\Delta(B_\perp) = (37.8\sqrt{B_\perp} + 0.15B_\perp)meV$ Fig.2. Here we have taken the bare value $\varepsilon_r = 1$ for suspended graphene. For the range of magnetic fields ($B \in (1,12)T$) our model gaps are 30-50% larger than the experimentally observed ones. This is a reasonable agreement considering our analysis does not include the effects of disorder and ignores the screening effects of the long-ranged Coulomb interactions, which is known to reduce the theoretical values of gaps of clean samples.

Reference [5] fits a straight line to the gap at $\sigma_H = 0$ for graphene on boron nitride substrates. While the fit to our model results does have a linear term, it is small and arises from our cut-off procedure. This experimental observation⁵ is hence not consistent with our model.

The tilted field measurements by Young et.al.⁵ show a decrease in the gaps with increasing tilt angle. The gaps vary linearly as a function of B_T (for fixed B_\perp). In Sec.VIII A we showed that there are three ground states in U - V parameter space: charge ordered, ferromagnetic and canted-spin state. The variation of particle-hole gaps w.r.t B_T for each ground state is shown in Fig.11b. The gaps for the ferromagnetic and canted-spin states increase with increasing B_T . Only the charge ordered state shows a linear decrease. Thus we conclude that the region labeled E_2 in Fig.11a demarcates the region in U - V consistent with experiments.

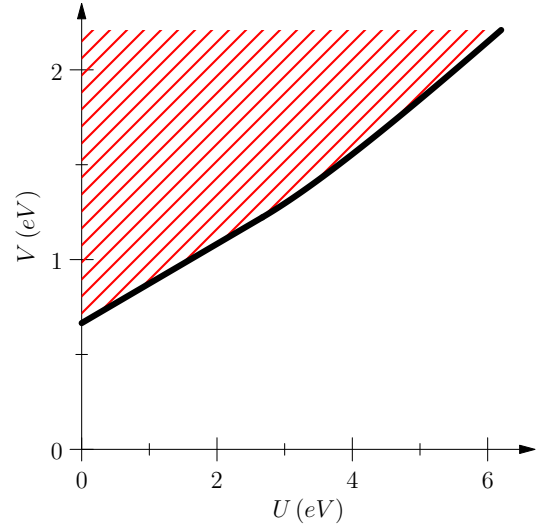


FIG. 13. The figure shows the delineated region in U - V parameter space that is consistent with excitations observed⁵ for the Hall conductivity at $\sigma_H = 0$ for graphene sample on boron nitride. The dashed area shown is the region where the gaps decrease with increasing B_T . The plot is shown for $B_\perp = 5T$ and $\varepsilon_r = 4.0$ for boron nitride substrate.

The gaps¹⁴ for $\sigma_H = -1$ were reported to be $\Delta_{\sigma_H=-1} = (8.5\sqrt{B} - 1.8)meV$. The large difference between the gaps at $\sigma_H = 0$ and $\sigma_H = -11$ strongly indicate skyrmionic excitations^{5,14} about the ground state at $\sigma_H = -1$. The values of our model gaps are the same at $\sigma_H = 0$ and $\sigma_H = -1$ since we compute the gaps for single quasi-particles and do not consider skyrmionic excitations. For this reason we do not compare our model results for the tilt angle dependence of the gaps with experimental observations.

To conclude, the behaviour of the quasi-particle gaps as a function of the tilt angle at $\sigma_H = 0$ is consistent with the experimental results in reference [5] in the region shown in Fig.13. This region has been computed for graphene on boron nitride, $\varepsilon_r = 4.0$.

X. SUMMARY

In this paper, we have investigated the role of the Dirac Sea and long-ranged Coulomb interactions in $SU(4)$ symmetry breaking in graphene. We have concentrated on the integer quantum Hall states in the vicinity of the charge neutral point.

We started with a realistic interacting lattice model for graphene. The model includes long-ranged Coulomb point-charge interactions and short ranged corrections to it. The short ranged corrections are parameterized by two phenomenological parameters U and V . We have presented a systematic derivation of the continuum limit of this lattice model. All our computations are done using this effective continuum theory.

We take a variational approach to the problem. We have developed a technique, using the heat kernel representation of the Dirac propagator in the presence of a magnetic field to make the computations of Coulomb energy of the Dirac sea tractable. Our variational wavefunctions allow for a staggered $SU(4)$ polarization of the Dirac sea. We show that this indeed happens and results in phases that are absent if the Dirac sea were ignored. The canted phase for $\sigma_H = 0$ and the valley-spin canted phase for $\sigma_H = -1$ were shown to be direct consequences of the inclusion of the filled Dirac sea in our calculations.

The ground state manifolds for $\sigma_H = 0$ and $\sigma_H = -1$ are the coset spaces $U(4)/(U(2) \times U(2))$ and $U(4)/(U(3) \times U(1))$ respectively. Thus there will be 8 gapless collective modes for $\sigma_H = 0$ and 6 for $\sigma_H = -1$. The explicit $SU(4)$ symmetry breaking terms, the short-ranged interactions and the Zeeman term, pick out specific ground states which depend on U and V . We have provided explicit parameterization of the ground state manifolds and have done a complete search to compute the phase diagram in U - V space. We find three phases at $\sigma_H = 0$ and two at $\sigma_H = -1$. The canted-spin state at $\sigma_H = 0$ and the valley-spin canted phase at $\sigma_H = -1$ have a remnant $U(1)$ degeneracy. In the other three cases the degeneracy is at most a discrete set. Thus we expect one Goldstone boson to remain gapless in the first two cases and all to get gapped in the other three phases.

A comparison of our model with tilted field experiments⁵ at $\sigma_H = 0$ shows that only the charge ordered phase is consistent with the observed behaviour of the gaps. This enables us to demarcate a region in U - V space consistent with experiments on graphene. This region is shown in Fig.13.

While we have only analyzed the symmetry breaking of the $n = 0$ integer quantum Hall states, our method is applicable to $n \neq 0$ also. We will be reporting on these cases in the near future.

ACKNOWLEDGMENTS

We acknowledge useful discussions with J.K. Jain and S.R. Hassan.

Appendix A: Heat kernel representation of two point correlation function

In this section, we evaluate the two point correlator using the time ordered Feynman propagator for a massive Dirac particle in the presence of a magnetic field. Consider a massive Dirac particle in $(2+1)d$ subjected to a magnetic field along the z -axis. The hamiltonian,

$$h = \frac{\hbar v_F}{\ell_c} \begin{pmatrix} m & \pi_x - i\pi_y \\ \pi_x + i\pi_y & -m \end{pmatrix}. \quad (A1)$$

Here $m > 0$ is expressed in units of $\hbar v_F/\ell_c$, and the eigenvalues are,

$$\begin{aligned} \epsilon_{n,l} &= \text{sgn}(n) \left(\frac{\hbar v_F}{\ell_c} \right) \sqrt{2|n| + m^2}. \\ \epsilon_{0,l} &= -m. \end{aligned} \quad (A2)$$

The completeness relation is,

$$\mathbb{1}_2 = \sum_{n=-\infty}^{\infty} \sum_{l=-|n|}^{\infty} \left(\Theta(-\epsilon_n) |n, l\rangle \langle n, l| + \Theta(\epsilon_n) |n, l\rangle \langle n, l| \right).$$

Here $\mathbb{1}_2$ is 2×2 identity matrix, $\epsilon_n > 0$ and the first term is a summation over all negative energy eigenvalue states which include all the Landau levels with negative indices and the $n = 0$ Landau level since the eigenvalue is $-m$ with $m > 0$. The second term is for states with positive energies i.e. Landau levels with indices $n > 0$.

We are interested in constructing the two point correlator,

$$G_{s,s'}(\mathbf{r}, \mathbf{r}_0) = \frac{1}{2} \langle 0 | [\Psi_s^\dagger(\mathbf{r}), \Psi_{s'}(\mathbf{r}_0)] | 0 \rangle. \quad (A3)$$

Here $|0\rangle$, the vacuum is constructed by occupying Landau levels with index $n = 0$ and $n < 0$ i.e. all the Landau levels with negative energy eigenvalues. This definition takes into account the subtraction of background charge from the positive charged ions.

$$G = \frac{1}{2} \sum_{n=-\infty}^{\infty} \sum_{l=-|n|}^{\infty} (\Theta(-\epsilon_n) - \Theta(\epsilon_n)) |n, l\rangle \langle n, l|. \quad (A4)$$

Let

$$K = \Theta(-\epsilon_n) - \Theta(\epsilon_n). \quad (A5)$$

K can be defined as following by considering equal time for the time ordered Feynman propagator,

$$K = \lim_{\tau \rightarrow 0^-} K(\tau) + \lim_{\tau \rightarrow 0^+} K(\tau). \quad (A6)$$

Here

$$K(\tau) = e^{-\tau \epsilon_n} \Theta(-\tau) \Theta(-\epsilon_n) - e^{-\tau \epsilon_n} \Theta(\tau) \Theta(\epsilon_n) \quad (A7)$$

$$= - \int_{-\infty}^{+\infty} \frac{d\omega}{2\pi} \frac{e^{i\omega\tau}}{\epsilon_n + i\omega}. \quad (A8)$$

We make use of the integral representation,

$$\frac{1}{\epsilon_n^2 + \omega^2} = \int_0^\infty ds e^{-s(\epsilon_n^2 + \omega^2)}. \quad (A9)$$

and evaluate the integrals and obtain the correlator for massive Dirac particle,

$$G = -\frac{1}{2\sqrt{\pi}} \int_0^\infty \frac{ds}{\sqrt{s}} h e^{-sh^2}. \quad (A10)$$

This is the so called ‘heat kernel’ representation.

To express the heat kernel operator in configuration space, we use the fact that \hbar^2 is diagonal. and from the knowledge of imaginary time, i.e. $t = -i\hbar\beta$, the propagator for the hamiltonian $(\pi_x^2 + \pi_y^2)(\hbar\omega_c/2)$ in configuration space¹⁸,

$$\begin{aligned} \sum_{n,l} \varphi_{n,l}^*(\mathbf{r}_0) e^{-\beta(\frac{\hbar\omega_c}{2})(\pi_x^2 + \pi_y^2)} \varphi_{n,l}(\mathbf{r}) \\ = \frac{1}{2\pi\ell_c^2} \frac{e^{-\frac{1}{4\ell_c^2}|\mathbf{r}-\mathbf{r}_0|^2 \coth(\frac{\beta\hbar\omega_c}{2})}}{2 \sinh(\frac{\beta\hbar\omega_c}{2})} e^{\frac{i}{2\ell_c^2}(xy_0 - yx_0)}. \end{aligned}$$

This enables us to write e^{-sh^2} in configuration space,

$$\langle \mathbf{r}_0 | e^{-sh^2} | \mathbf{r} \rangle = \frac{1}{2\pi\ell_c^2} \zeta_s(\mathbf{r}, \mathbf{r}_0) \frac{e^{-sm^2}}{2 \sinh(s)} \begin{pmatrix} e^{-s} & 0 \\ 0 & e^s \end{pmatrix}. \quad (\text{A11})$$

here,

$$\zeta_s(\mathbf{r}, \mathbf{r}_0) = e^{-\frac{1}{4}|\mathbf{r}-\mathbf{r}_0|^2 \coth(s)} e^{\frac{i}{2}(xy_0 - yx_0)}. \quad (\text{A12})$$

Since s has dimension of the inverse of the square energy and \mathbf{r} has the dimension of length,

$$\frac{s}{\epsilon^2} \rightarrow s, \quad \frac{\mathbf{r}}{\ell_c} \rightarrow \mathbf{r}.$$

To obtain the propagator, we need to evaluate $\hbar e^{-sh^2}$. This is achieved by finding the action of operators π_+ and π_- on $\zeta_s(\mathbf{r}, \mathbf{r}_0)$. To accomplish this we express the operators π_{\pm} in terms of the complex variable $z = x + iy$ and its conjugate \bar{z} . We have to take into account the ultra-violet cut-off because of the underlying lattice structure of graphene. This is taken into account by taking the limits of integration from $1/2N_C$ to infinity for s variable in Eq.(A10). In configuration space the equal time two point correlator, $\langle \mathbf{r}_2 | G | \mathbf{r}_1 \rangle = G_m(\mathbf{r}_1, \mathbf{r}_2)$

$$G_m(\mathbf{r}_1, \mathbf{r}_2) = \frac{1}{2} \frac{1}{2\pi\ell_c^2} \begin{pmatrix} -f_m(\mathbf{r}_1, \mathbf{r}_2) & d_m(\mathbf{r}_1, \mathbf{r}_2) \\ b_m(\mathbf{r}_1, \mathbf{r}_2) & g_m(\mathbf{r}_1, \mathbf{r}_2) \end{pmatrix}. \quad (\text{A13})$$

Here,

$$f_m(\mathbf{r}_1, \mathbf{r}_2) = \frac{m}{2\sqrt{\pi}} \int_{\frac{1}{2N_C}}^{\infty} \frac{ds}{\sqrt{s}} \frac{e^{-s(m^2+1)}}{\sinh(s)} \zeta_s(\mathbf{r}_1, \mathbf{r}_2). \quad (\text{A14})$$

$$g_m(\mathbf{r}_1, \mathbf{r}_2) = \frac{m}{2\sqrt{\pi}} \int_{\frac{1}{2N_C}}^{\infty} \frac{ds}{\sqrt{s}} \frac{e^{-s(m^2-1)}}{\sinh(s)} \zeta_s(\mathbf{r}_1, \mathbf{r}_2). \quad (\text{A15})$$

$$b_m(\mathbf{r}_1, \mathbf{r}_2) = -i \frac{(z_1 - z_2)}{4\sqrt{\pi}} \int_{\frac{1}{2N_C}}^{\infty} \frac{ds}{\sqrt{s}} \frac{e^{-sm^2}}{\sinh^2(s)} \zeta_s(\mathbf{r}_1, \mathbf{r}_2). \quad (\text{A16})$$

$$d_m(\mathbf{r}_1, \mathbf{r}_2) = -i \frac{(\bar{z}_1 - \bar{z}_2)}{4\sqrt{\pi}} \int_{\frac{1}{2N_C}}^{\infty} \frac{ds}{\sqrt{s}} \frac{e^{-sm^2}}{\sinh^2(s)} \zeta_s(\mathbf{r}_1, \mathbf{r}_2). \quad (\text{A17})$$

Appendix B: Variational state energy for symmetric model

1. Kinetic term

The kinetic term has local fermion field operators and the expectation value can be expressed as,

$$\langle \mathcal{H}_t \rangle = \kappa_t \int_{\mathbf{r}} h_{r,A;s,B} \langle \Psi_{r,A}^\dagger(\mathbf{r}) \Psi_{s,B}(\mathbf{r}) \rangle. \quad (\text{B1})$$

Here $h_{r,A;s,B} = (\boldsymbol{\alpha} \cdot \boldsymbol{\pi})_{r,s} (\mathbb{1}_4)_{A,B}$. To compute the average of kinetic term we need to take into account the action of the operator \hbar which makes it non-local because of the action of conjugate momentum operator. We cannot apply the coincident correlator here, instead we compute the action of the operator \hbar on the two point correlator and take the coincident limit.

$$\langle \mathcal{H}_t \rangle = \kappa_t \lim_{\mathbf{r} \rightarrow \mathbf{r}_0} \text{Tr}[\hbar \Gamma(\mathbf{r}, \mathbf{r}_0)]. \quad (\text{B2})$$

The operator $\boldsymbol{\alpha} \cdot \boldsymbol{\pi}$ has only off-diagonal elements, hence

$$\begin{aligned} \text{Tr}[\hbar \Gamma(\mathbf{r}, \mathbf{r}_0)] &= \frac{1}{2\pi} \frac{\kappa_t}{2} \sum_{q=1}^4 (\pi_- b_{m_q}(\mathbf{r}, \mathbf{r}_0) \\ &\quad + \pi_+ d_{m_q}(\mathbf{r}, \mathbf{r}_0)). \end{aligned} \quad (\text{B3})$$

Here $\pi_{\pm} = \pi_x \pm i\pi_y$, we obtain

$$\begin{aligned} \lim_{\mathbf{r} \rightarrow \mathbf{r}_0} \pi_- b_{m_q}(\mathbf{r}, \mathbf{r}_0) &= \lim_{\mathbf{r} \rightarrow \mathbf{r}_0} \pi_+ d_{m_q}(\mathbf{r}, \mathbf{r}_0) \\ &= -\frac{1}{2\sqrt{\pi}} \int_s \frac{e^{-sm_q^2}}{\sqrt{s} \sinh^2(s)}. \end{aligned} \quad (\text{B4})$$

The spatial integration in Eq.(B1) is trivial and results in the volume of the system. The kinetic energy density,

$$\mathcal{E}_t = -\frac{\kappa_t}{2\pi} \frac{1}{2\sqrt{\pi}} \sum_{q=1}^4 \int_{\frac{1}{2N_C}}^{\infty} ds \frac{e^{-sm_q^2}}{\sqrt{s} \sinh^2(s)}. \quad (\text{B5})$$

The integrand in Eq.(B5), is a diverging function of s near zero. We note that leading contribution of this integration is independent of variational parameters, which is just a constant from the minimization point of view. So we drop this constant in the process of computing the coefficients with variational parameter dependence. The kinetic term density that has variational parameter dependence can be expressed as,

$$\mathcal{E}_t = \kappa_t \sum_{q=1}^4 \eta_t(m_q^2). \quad (\text{B6})$$

The quantity

$$\eta_t(m_q^2) = \frac{1}{2\sqrt{\pi}} \int_{\frac{1}{2N_C}}^{\infty} ds \frac{(1 - e^{-sm_q^2})}{\sqrt{s} \sinh^2(s)}. \quad (\text{B7})$$

The coefficient $\eta_t(m_q^2)$ always yields positive values for the range of integration and parameter values that are of our interest.

2. Coulomb interaction term

The variational state energy contributions from the Coulomb term come from the exchange term and can be expressed in terms of the two point correlator,

$$\langle \mathcal{H}_C \rangle = -\kappa_C \iint_{\mathbf{r}_1, \mathbf{r}_2} \frac{1}{|\mathbf{r}|} \text{Tr}[\Gamma(\mathbf{r}_1, \mathbf{r}_2) \Gamma(\mathbf{r}_2, \mathbf{r}_1)]. \quad (\text{B8})$$

Here $|\mathbf{r}| = |\mathbf{r}_1 - \mathbf{r}_2|$. We use the fact, $\text{Tr}[P_q P_{\tilde{q}}] = \delta_{q, \tilde{q}}$, to evaluate the trace of the correlator, This indicated that the Coulomb expectation value is independent of the angle parameters.

Now consider the integral

$$\mathcal{I}_1 = \frac{1}{(2\pi)^2} \frac{1}{4} \iint_{\mathbf{r}_1, \mathbf{r}_2} \frac{1}{|\mathbf{r}|} \left(f_{m_q}(\mathbf{r}_1, \mathbf{r}_2) f_{m_q}(\mathbf{r}_2, \mathbf{r}_1) + g_{m_q}(\mathbf{r}_2, \mathbf{r}_1) g_{m_q}(\mathbf{r}_1, \mathbf{r}_2) \right). \quad (\text{B9})$$

Once again we plug in $f_{m_q}(\mathbf{r}_1, \mathbf{r}_2)$ from Eq.(A14) and $g_{m_q}(\mathbf{r}_1, \mathbf{r}_2)$ from Eq.(A15) in the above equation,

$$\mathcal{I}_1 = \frac{1}{(2\pi)^2} \frac{m_q^2}{8\pi} \iint_{s_1, s_2} \frac{e^{-(s_1+s_2)m_q^2} \cosh(s_1 + s_2)}{\sqrt{s_1 s_2} \sinh(s_1) \sinh(s_2)} \iint_{\mathbf{r}_1, \mathbf{r}_2} \frac{e^{-\frac{1}{4}|\mathbf{r}|^2(\coth(s_1)+\coth(s_2))}}{|\mathbf{r}|}. \quad (\text{B10})$$

The spatial integration involves only the magnitude of the relative position coordinates, hence we transform the spatial integration from two position coordinates to the center of mass and the relative coordinates. The center of mass coordinate is trivial and yields the volume of the system and the relative coordinate is a gaussian integral.

$$\mathcal{I}_1 = \frac{V}{2\pi} \eta_{fg}(m_q^2). \quad (\text{B11})$$

$$\eta_{fg}(m_q^2) = \frac{m_q^2}{8\sqrt{\pi}} \iint_{s_1, s_2} \frac{e^{-(s_1+s_2)m_q^2}}{\sqrt{s_1 s_2}} \frac{\cosh(s_1 + s_2)}{\sqrt{\sinh(s_1) \sinh(s_2) \sinh(s_1 + s_2)}}. \quad (\text{B12})$$

Now consider the integral,

$$\mathcal{I}_2 = \frac{1}{(2\pi)^2} \frac{1}{4} \iint_{\mathbf{r}_1, \mathbf{r}_2} \frac{1}{|\mathbf{r}|} \left(b_{m_q}(\mathbf{r}_1, \mathbf{r}_2) d_{m_q}(\mathbf{r}_2, \mathbf{r}_1) + b_{m_q}(\mathbf{r}_2, \mathbf{r}_1) d_{m_q}(\mathbf{r}_1, \mathbf{r}_2) \right). \quad (\text{B13})$$

Taking $b_{m_q}(\mathbf{r}_1, \mathbf{r}_2)$ from Eq.(A16) and $d_{m_q}(\mathbf{r}_1, \mathbf{r}_2)$ from Eq.(A17) and plugging in the above equation,

$$\mathcal{I}_2 = \frac{1}{(2\pi)^2} \frac{1}{32\pi} \iint_{s_1, s_2} \frac{e^{-s_1 m_q^2}}{\sqrt{s_1} \sinh^2(s_1)} \frac{e^{-s_2 m_q^2}}{\sqrt{s_2} \sinh^2(s_2)} \iint_{\mathbf{r}_1, \mathbf{r}_2} |\mathbf{r}| e^{-\frac{1}{4}|\mathbf{r}|^2(\coth(s_1)+\coth(s_2))}. \quad (\text{B14})$$

Once again the spatial integration is done by transforming to the center of mass and relative coordinates and is done analytically using gamma functions. The integrand has a leading contribution independent of variational parameter, a similar situation was seen in the computation of the expectation value of the kinetic term. We drop the contributions that are independent of the variational parameter,

$$\mathcal{I}_2 = \frac{V}{2\pi \ell_c^2} \eta_{bd}(m_q^2). \quad (\text{B15})$$

$$\eta_{bd}(m_q^2) = \iint_{s_1, s_2} \frac{(e^{-(s_1+s_2)m_q^2} - 1)}{\sqrt{s_1} \sqrt{s_2} \sinh^2(s_1) \sinh^2(s_2)} \frac{1}{(\coth(s_1) + \coth(s_2))^{\frac{3}{2}}}. \quad (\text{B16})$$

The net variational parameter dependence of Coulomb term energy density is expressed as,

$$\mathcal{E}_C = \frac{1}{2\pi} \kappa_C \sum_{q=1}^4 \eta_{C_2}(m_q^2). \quad (\text{B17})$$

where

$$\eta_{C_2}(m_q^2) = \eta_{fg}(m_q^2) + \eta_{bd}(m_q^2). \quad (\text{B18})$$

Appendix C: Order parameters and lattice dictionary

In this section, we provide the simplest lattice representation for the 32 order parameters discussed in Sec.III B. The lattice vectors for the nearest neighbour sites are: $\mathbf{b}_1 = 0$, $\mathbf{b}_2 = \mathbf{e}_2$, $\mathbf{b}_3 = \mathbf{e}_1 + \mathbf{e}_2$, and the next nearest neighbour vectors are: $\mathbf{a}_1 = \mathbf{e}_1$, $\mathbf{a}_2 = \mathbf{e}_2$, $\mathbf{a}_3 = \mathbf{e}_1 + \mathbf{e}_2$. The table lists the order parameters and the corresponding lattice representation. Here σ^ν are 2×2 identity and Pauli matrices for index $\nu = 0, x, y, z$ respectively.

Order parameter	Lattice operator
$\mathcal{T}^{0\nu}(\mathbf{x})$	$\left(c_{1,\mathbf{n}}^\dagger \sigma^\nu c_{1,\mathbf{n}} + c_{2,\mathbf{n}}^\dagger \sigma^\nu c_{2,\mathbf{n}}\right) + \text{h.c}$
$\mathcal{T}^{3\nu}(\mathbf{x})$	$-i \left(c_{1,\mathbf{n}}^\dagger \sigma^\nu \left(\sum_{j=1}^3 c_{1,\mathbf{n}+\mathbf{a}_j} \right) + c_{2,\mathbf{n}}^\dagger \sigma^\nu \left(\sum_{j=1}^3 c_{2,\mathbf{n}+\mathbf{a}_j} \right) \right) + \text{h.c}$
$\mathcal{T}^{1\nu}(\mathbf{x})$	$\left(e^{i\mathbf{K}_+\cdot\mathbf{n}} c_{\mathbf{n},1}^\dagger \sigma^\nu \sum_{j=1}^3 e^{-i\mathbf{K}_-\cdot(\mathbf{n}+\mathbf{b}_j)} c_{\mathbf{n}+\mathbf{b}_j,2} - e^{-i\mathbf{K}_+\cdot\mathbf{n}} c_{\mathbf{n},1}^\dagger \sigma^\nu \sum_{j=1}^3 e^{i\mathbf{K}_-\cdot(\mathbf{n}+\mathbf{b}_j)} c_{\mathbf{n}+\mathbf{b}_j,2} \right) + \text{h.c}$
$\mathcal{T}^{2\nu}(\mathbf{x})$	$-i \left(e^{i\mathbf{K}_+\cdot\mathbf{n}} c_{\mathbf{n},1}^\dagger \sigma^\nu \sum_{j=1}^3 e^{-i\mathbf{K}_-\cdot(\mathbf{n}+\mathbf{b}_j)} c_{\mathbf{n}+\mathbf{b}_j,2} - e^{-i\mathbf{K}_+\cdot\mathbf{n}} c_{\mathbf{n},1}^\dagger \sigma^\nu \sum_{j=1}^3 e^{i\mathbf{K}_-\cdot(\mathbf{n}+\mathbf{b}_j)} c_{\mathbf{n}+\mathbf{b}_j,2} \right) + \text{h.c}$
$\tilde{\mathcal{T}}^{0\nu}(\mathbf{x})$	$-i \left(c_{1,\mathbf{n}}^\dagger \sigma^\nu \left(\sum_{j=1}^3 c_{1,\mathbf{n}+\mathbf{a}_j} \right) - c_{2,\mathbf{n}}^\dagger \sigma^\nu \left(\sum_{j=1}^3 c_{2,\mathbf{n}+\mathbf{a}_j} \right) \right) - \text{h.c}$
$\tilde{\mathcal{T}}^{3\nu}(\mathbf{x})$	$\left(c_{\mathbf{n},1}^\dagger \sigma^\nu c_{\mathbf{n},1} - c_{\mathbf{n},2}^\dagger \sigma^\nu c_{\mathbf{n},2} \right) + \text{h.c}$
$\tilde{\mathcal{T}}^{1\nu}(\mathbf{x})$	$\left(e^{i\mathbf{K}_+\cdot\mathbf{n}} c_{\mathbf{n},1}^\dagger \sigma^\nu \sum_{j=1}^3 e^{-i\mathbf{K}_-\cdot(\mathbf{n}+\mathbf{b}_j)} c_{\mathbf{n}+\mathbf{b}_j,2} + e^{-i\mathbf{K}_+\cdot\mathbf{n}} c_{\mathbf{n},1}^\dagger \sigma^\nu \sum_{j=1}^3 e^{i\mathbf{K}_-\cdot(\mathbf{n}+\mathbf{b}_j)} c_{\mathbf{n}+\mathbf{b}_j,2} \right) + \text{h.c}$
$\tilde{\mathcal{T}}^{2\nu}(\mathbf{x})$	$-i \left(e^{i\mathbf{K}_+\cdot\mathbf{n}} c_{\mathbf{n},1}^\dagger \sigma^\nu \sum_{j=1}^3 e^{-i\mathbf{K}_-\cdot(\mathbf{n}+\mathbf{b}_j)} c_{\mathbf{n}+\mathbf{b}_j,2} + e^{-i\mathbf{K}_+\cdot\mathbf{n}} c_{\mathbf{n},1}^\dagger \sigma^\nu \sum_{j=1}^3 e^{i\mathbf{K}_-\cdot(\mathbf{n}+\mathbf{b}_j)} c_{\mathbf{n}+\mathbf{b}_j,2} \right) + \text{h.c}$

* vinu@imsc.res.in

† shankar@imsc.res.in

¹ K. S. Novoselov, D. Jiang, F. Schedin, T. J. Booth, V. V. Khotkevich, S. V. Morozov, and A. K. Geim, Proceedings of the National Academy of Sciences of the United States of America **102**, 10451 (2005).² V. P. Gusynin and S. G. Sharapov, Phys. Rev. Lett. **95**, 146801 (2005).³ K. Novoselov, A. Geim, S. Morozov, D. Jiang, M. I. Katsnelson, I. V. Grigorieva, S. V. Dubonos, and A. Firsov, Nature **438**, 197 (2005).⁴ Y. Zhang, Y.-W. Tan, H. L. Stormer, and P. Kim, Nature **438**, 201 (2005).⁵ A. F. Young, C. R. Dean, L. Wang, H. Ren, P. Cadden-Zimansky, K. Watanabe, T. Taniguchi, J. Hone, K. L. Shepard, and P. Kim, Nat Phys **8**, 550 (2012).⁶ K. Nomura and A. H. MacDonald, Phys. Rev. Lett. **96**, 256602 (2006).⁷ K. Yang, S. Das Sarma, and A. H. MacDonald, Phys. Rev. B **74**, 075423 (2006).⁸ J. Alicea and M. P. A. Fisher, Phys. Rev. B **74**, 075422 (2006).⁹ V. P. Gusynin, V. A. Miransky, S. G. Sharapov, and I. A. Shovkovy, Phys. Rev. B **74**, 195429 (2006).¹⁰ J.-N. Fuchs and P. Lederer, Phys. Rev. Lett. **98**, 016803 (2007).¹¹ M. O. Goerbig, R. Moessner, and B. Douçot, Phys. Rev. B **74**, 161407 (2006).¹² I. F. Herbut, Phys. Rev. B **75**, 165411 (2007).¹³ M. Kharitonov, Phys. Rev. B **85**, 155439 (2012).¹⁴ D. A. Abanin, B. E. Feldman, A. Yacoby, and B. I. Halperin, Phys. Rev. B **88**, 115407 (2013).¹⁵ J. Jung and A. H. MacDonald, Phys. Rev. B **80**, 235417 (2009).¹⁶ I. F. Herbut, Phys. Rev. B **76**, 085432 (2007).¹⁷ F. D. M. Haldane, Phys. Rev. Lett. **61**, 2015 (1988).¹⁸ M. L. Glasser, Phys. Rev. **133**, B831 (1964).